Semiconducting Thienothiophene Copolymers: Design, Synthesis, Morphology, and Performance in Thin-Film Organic Transistors

By *Iain McCulloch,* Martin Heeney,* Michael L. Chabinyc,* Dean DeLongchamp,* R. Joseph Kline, Michael Cölle, Warren Duffy, Daniel Fischer, David Gundlach, Behrang Hamadani, Rick Hamilton, Lee Richter, Alberto Salleo, Maxim Shkunov, David Sparrowe, Steven Tierney,* and *Weimin Zhang*

Organic semiconductors are emerging as a viable alternative to amorphous silicon in a range of thin-film transistor devices. With the possibility to formulate these p-type materials as inks and subsequently print into patterned devices, organic-based transistors offer significant commercial advantages for manufacture, with initial applications such as low performance displays and simple logic being envisaged. Previous limitations of both air stability and electrical performance are now being overcome with a range of both small molecule and polymer-based solution-processable materials, which achieve charge carrier mobilities in excess of 0.5 $cm^2 V^{-1} s^{-1}$, a benchmark value for amorphous silicon semiconductors. Polymer semiconductors based on thienothiophene copolymers have achieved amongst the highest charge carrier mobilities in solution-processed transistor devices. In this Progress Report, we evaluate the advances and limitations of this class of polymer in transistor devices.

1. Introduction

Transistors are employed as the switching or amplifying components of almost all forms of integrated circuitry, and are the key element of modern electronics.[1] Manufacture involves material deposition and patterning using a series of high-temperature, high-vacuum processes with lithographic patterning and mask steps. Although the high circuit density makes the cost per transistor extremely low, the cost per unit area remains high, and alternative processing and new materials have been a focus for cost reduction and ease of processing, especially at large areas.[2–4] Migrating to flexible circuitry will likely require lower processing temperatures, compatible with plastic substrates additionally driving the introduction of new materials.[5] To accommodate these requirements, transistors composed of organic semiconductors, which can be printed from solution, have emerged as a promising possibility.[6–9] Organic transistors are typically p-type field-effect devices, operating in the accumulation mode. Holes are injected into the highest occupied molecular orbital (HOMO) energy level of the organic semiconductor and can be transported between the source and drain electrodes, modulated by the gate electrode, which is insulated from the accumulation channel by an organic dielectric layer. The

[*] Prof. I. McCulloch, Dr. R. Hamilton
Department of Chemistry
Imperial College, London, SW7 2AZ (UK)
E-mail: iain.mcculloch@imperial.ac.uk
Dr. M. Heeney
Department of Materials
Queen Mary University of London, London, E1 4NS (UK)
E-mail: m.heeney@qmul.ac.uk
Prof. M. L. Chabinyc
University of California, Santa Barbara, 93106-5050 (USA)
E-mail: mchabinyc@engineering.ucsb.edu
Dr. D. DeLongchamp, Dr. R. J. Kline, Dr. D. Fischer, Dr. D. Gundlach, Dr. B. Hamadani, Dr. L. Richter
National Institute of Standards and Technology
Gaithersburg, MD 20899 (USA)
E-mail: dean.delongchamp@nist.gov
Dr. M. Cölle, Dr. W. Duffy, Dr. D. Sparrowe, Dr. S. Tierney, Dr. W. Zhang
Merck Chemicals
Chilworth Science Park, Southampton, SO167QD (UK)
Prof. A. Salleo
Stanford University, Palo Alto, CA 94305 (USA)
Dr. M. Shkunov
University of Surrey, Guilford, GU2 7XH (UK)

DOI: 10.1002/adma.200801650

Iain McCulloch is Professor of Polymer Materials in the Department of Chemistry at Imperial College London and co-founder of Flexink Ltd. His research interests are in the design, synthesis, and application of conjugated materials for optical and electronic applications. He obtained a PhD in Polymer Chemistry in 1989 at the University of Strathclyde, then joined Hoechst Celanese to engage in the research of novel functional polymers for nonlinear optics, lithography, and drug delivery. He was a Research Manager at Merck Chemicals from 2000 to 2007, responsible for novel organic semiconductor materials for application in organic field-effect transistors and photovoltaic devices.

Martin Heeney is a senior lecturer in the Materials Department at Queen Mary University of London. He obtained his PhD in chemistry from the University of East Anglia (1999). Prior to his current appointment, he was the chemistry team leader for the organic electronics group at Merck Chemical. His research interests include the development and characterization of novel materials for a variety of optoelectronic and sensing applications. He is co-founder and director of Flexink Ltd., a technology start-up company commercializing organic semiconductor materials.

Michael L. Chabinyc is an Associate Professor in the Materials Department at the University of California, Santa Barbara. He received his Ph.D. in chemistry from Stanford University (1999) and was an N.I.H. post-doctoral fellow at Harvard University (2001). He was a senior research staff member in the Electronic Materials and Devices Laboratory at Palo Alto Research Center before moving to UCSB. His current research focuses on semiconducting polymers for printed electronics and energy conversion.

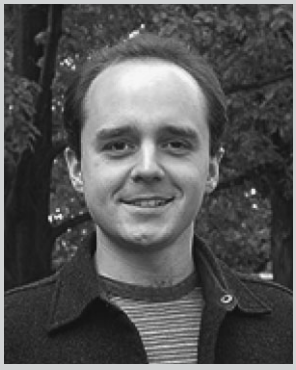

Dean M. DeLongchamp leads the Organic Electronics and Photovoltaics project in the Polymers Division at the National Institute of Standards and Technology (NIST). He received a Ph. D. in Chemical Engineering from MIT in 2003 for the development of functional self-assembled polymer films with applications in displays, batteries, and fuel cells. His current research is focused on understanding the relationship between device function and nanoscale interfacial structure at organic semiconductor interfaces with advanced measurement methods such as soft X-ray spectroscopy and neutron reflectivity.

electrical performance of the transistor is typically described in terms of the semiconductor charge carrier mobility and the current ON/OFF ratio. Both the current that can be delivered by the transistor and the charging speed depend on the semiconductor charge carrier mobility, and each application will have a minimum mobility requirement for optimal operation.[6,10] Low-performance displays are likely to be the first application for organic transistors, particularly electrophoretic displays on plastic substrates,[11] with low-resolution and sub-video refresh rates. As the electrophoretic display effect is reflective, the transistor can occupy a large fraction of the area underneath the pixel electrode area, thus enabling larger transistor electrode widths (W) and correspondingly larger currents, hence requiring lower charge carrier mobilities, which are further relaxed by the low display refresh rates. Indeed, early products have mobility requirements of lower than $0.1\,cm^2\ V^{-1}\ s^{-1}$, well within the capability of both small molecule and polymer semiconductors. Although early applications can be served by currently available semiconductor materials, future demand for more complex and higher performing circuitry, enabling high-resolution, video-rate displays will require organic semiconductors with improved charge carrier mobility.[12] Both small molecule and polymer semiconductor transistors have been shown to depend on achieving a highly crystalline thin-film microstructure, with crystalline domains well connected and aligned together. Within the domains the semiconductor molecules pack closely together with their π conjugated aromatic rings linked in a planar conformation, allowing efficient intermolecular charge transfer. Successful organic transistors must be reliable over the lifetime of the application, and therefore good environmental stability is required. Most organic p-type semiconductors have electron-rich HOMO energy levels and often exhibit oxidative doping in the presence of ambient air and humidity. Current challenges are therefore to achieve both excellent electrical performance combined with ambient stability. While the charge carrier mobility in organic semiconductors is considered to be dependent on its molecular organization at the interface with the dielectric, it has also been shown to be manipulated by variables such as the polarity of the dielectric interface,[13,14] the electrical field across the accumulation channel,[15,16] and the work function of the injecting electrodes.[17] Thus, it can be considered to be a figure of merit related to the transistor configuration as much as an intrinsic property of the semiconductor. Standardizing device architecture and measurement technique is therefore important for accurate comparisons to be obtained between semiconductor materials. Both solution-processable small molecule and polymer semiconductors have been widely developed, and in both cases high mobility transistors have been achieved. The focus of this report is to review the design, characterization, and optimization of thienothiophene copolymers, a promising class of solution-processable organic semiconductor, and their application in transistor devices.

2. Polymer Semiconductors

Polymeric semiconductors typically comprise coupled aromatic monomer units, with extended π orbital conjugation along the length of the backbone. Solubility is induced through the attachment of aliphatic side units projecting from the backbone, giving rise to the term ''hairy rod'' to describe polymer conformation. Both the polymer molecular weight and polydispersity are important properties to optimize, as they influence the formulation rheology, as well as the thin film formation and morphology from solution printing or casting. Low molecular weight polymer can often arise from both unoptimized synthetic processes as well as low levels of solubility in polymerization solvents, and thus resulting in precipitation from solution and preventing extended chain growth. As the thermal properties and crystallinity are sensitive to molecular weight in the low molecular weight regime, it is also necessary to ensure that the molecular weight is above a rough threshold value beyond which point the physical properties tend to stabilize. This value is likely to be polymer-specific, but for most thiophene ''hairy rod'' polymers, a number average molecular weight value of about 20 kDa is a reasonable estimate of this threshold.[18] A motivating feature for the use of polymer materials, are that they can be solution coated into cohesive and conformal thin films. Control of film thickness and morphology can be achieved by optimization of solution rheology and thermal properties. Fabrication of multilayer stacks from solution deposition processes requires that each layer deposited is inert to the solvents and temperatures that it is subsequently exposed to during manufacture of the device. The narrow solubility parameter window of polymers, and their high bulk viscosity, typically increases the orthogonality options for solution deposition on top of polymer layers, thus expanding the choice of materials that can be used in devices. With negligible vapor pressure, polymers are not susceptible to interlayer diffusion during the typical device-fabrication thermal cycles, and typically exhibit robust mechanical properties, making thin semiconductor films potentially compatible with flexible processing or rollable substrate operation. As typical polymer crystalline domain sizes are much smaller that the length scale of the transistor channel dimensions, relatively isotropic in-plane transport occurs in transistor devices. This results in low device-to-device performance variability, which is particularly important where a larger number of transistors are required to be integrated.

3. Polythiophenes

Thiophene-containing polymers have exhibited amongst the highest charge carrier mobilities from field-effect transistors fabricated by solution deposition.[19–21] When thiophenes are coupled together in their 2^{nd} and 5^{th} positions, an extended delocalized electronic orbital system can be achieved in which the electron-rich thiophene rings are conjugated together and exhibit a coplanar conformation. This conformation provides the molecular template for achieving a highly crystalline thin-film microstructure, which plays a role in their excellent charge transport properties. The first semiconducting polymer to exhibit charge carrier mobilities in the $0.1\,cm^2\ V^{-1}\ s^{-1}$ range was regioregular poly(3-hexylthiophene) (P3HT)[20] which was found to be essential to achieve a highly crystalline microstructure and good electrical performance. P3HT has emerged as a benchmark semiconducting polymer due to its ready availability and ease of

processing from solution into highly crystalline thin-film microstructures. The molecular structure of this polymer is characterized by an alternating head-to-tail side chain regiopositioning along the backbone. The impact of the P3HT semiconductor microstructure on transistor device electrical performance has provided critical guidance for the design of new polymers that can replicate or even improve on these highly ordered thin films. From a design perspective, there are three fundamental weaknesses in these alkylthiophene polymers. Firstly, the monomer is non-centrosymmetric. This limits the range of polymerization techniques[22,23] that can be used to construct highly regular repeat units, which are necessary for highly crystalline thin films, but also introduces the concern of batch-to-batch variability. Secondly, the delocalized π electron system is very electron rich, which renders the polymer susceptible to a range of oxidation mechanisms.[24] Thirdly, the high side-chain density prevents side-chain interdigitation and ordering, thus reducing the extent of long-range intermolecular organization.[25] Thienothiophene copolymers were therefore designed in response to these limitations in conventional thiophene polymer molecular structure.

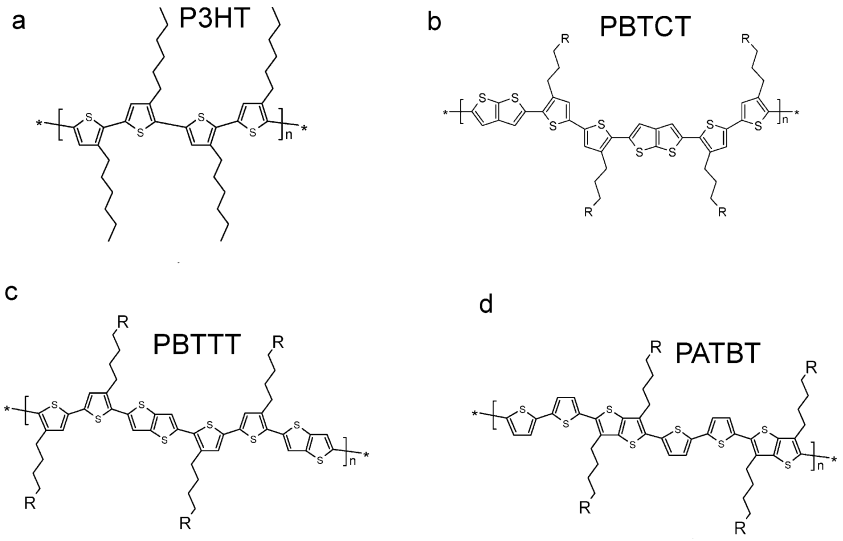

Figure 1. Extended backbone molecular structure of a) poly(3-hexylthiophene) (P3HT), b) poly(2,5-bis(3-alkylthiophen-2-yl)thieno[2,3-b]thiophene) (pBTCT), c) poly(2,5-bis(3-alkylthiophen-2-yl)thieno[3,2-b]thiophene) (pBTTT), and d) Poly(3,6-dialkylthieno[3,2-b]thiophene-co-bithiophene) (pATBT).

4. Thienothiophene Polymers

4.1. pBTCT

The main concept in the design of alternating copolymers of thieno[2,3-b]thiophene and 4,4′-dialkyl-2,2′-bithiophene **8**, referred to as pBTCT (poly(Bithiophene-crossconjugated thiophene) thieno[2,3-b]thiophene polymers,[26] illustrated in Figure 1b, is that the central cross-conjugated double bond of the thieno[2,3-b]thiophene unit prevents a fully conjugated pathway between substituents at the 2nd and 5th positions. Full delocalization of the conjugated π electron system along the backbone is therefore disfavored by the incorporation of this unit[27] and thus these polymers exhibit lower lying HOMO energy levels (corresponding to larger ionization potentials) than fully conjugated, planar thiophene polymers. Confirmation of this increased ionization potential was obtained from UPS measurements of thin films of a range of thiophene polymers including pBTCT, shown in Figure 2, where pBTCT has a 0.4 eV larger ionization potential than P3HT, mainly due to this reduced conjugation, although the reduced number of electron-donating alkyl chains per aromatic group also contributes. The backbone repeat unit was also designed to be regiosymmetrical. This ensures that the polymer does not exhibit regioisomerism, which can generate conformational irregularities, and reduce crystallinity. The most energetically favorable backbone conformation for these polymers requires that, where possible, the sulphurs in adjacent monomer units arrange in an ''anti'' configuration in order to maximize their spatial separation due to their large size. A consequence of this conformation is that the pBTCT polymer long axis has a ''crank-shaft'' like shape, and 2 different side-chain separation distances, as shown in Figure 1b. These distances are wide enough to enable the opportunity for side-chain interdigitation between neighboring polymer chains, however the lack of side-chain spacing symmetry may contribute to a suboptimal crystalline microstructure. As the thieno[2,3-b]thiophene monomer unit is planar, pBTCT can adopt a coplanar conformation, with a tail-to-tail regiosymmetrical arrangement of the alkyl chains of the thiophene units of the bithiophene monomer. This

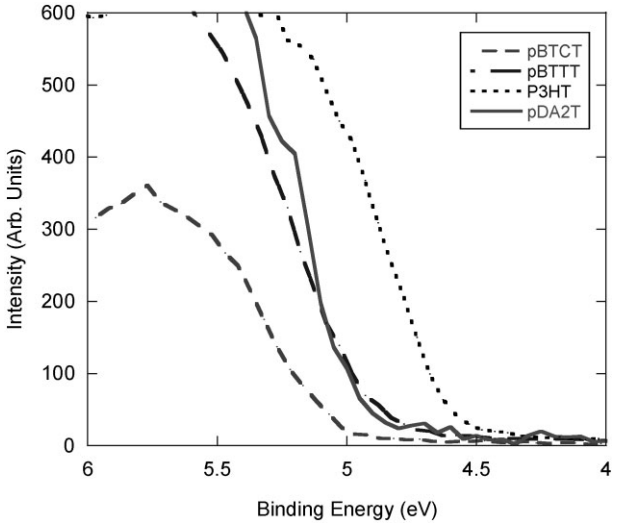

Figure 2. The low binding energy portion, of a UPS spectrum of thin semiconductor films, plotted versus intensity in arbitrary units (courtesy of W. Osikowicz and W. Salaneck, U. Linkoping, Sweden).

regiopositioning of the alkyl groups ensures that there are no steric interactions between neighboring alkyl chains, facilitating a highly planar backbone conformation and optimal π orbital overlap and delocalization within the bithiophene. In contrast, head-to-head regio-positioning would lead to significant steric interactions between the alkyl chains, promoting a resultant twist between the planes of adjacent thiophene rings.[28,29]

4.2. pBTTT

Poly(2,5-Bis(3-alkylthiophen-2-yl)thieno[3,2-b]thiophene (pBTTT) **1** illustrated in Figure 1c, is an alternating copolymer of thieno[3,2-b]thiophene and 4,4-dialkyl 2,2-bithiophene monomer units.[30] In contrast to pBTCT polymers, the thieno[3,2-b]thiophene monomer allows conjugation between adjacent thiophenes coupled in the 2nd and 5th positions, as it has a different arrangement of the double bonds within the fused ring, from the ''anti'' positioning of the sulfur atoms, compared to the ''syn'' positioning in thieno[2,3-b]thiophene. PBTTT therefore has extended π-orbital delocalization with correspondingly lower bandgap, and an ionization potential than pBTCT, as shown in Figure 2. In common with the pBTCT polymer series, the alkyl groups on the bithiophene act as the weakly inductive sigma electron donators into π electron systems. Reduction in the number of alkyl substituents on a conjugated thiophene polymer backbone will therefore increase the ionization potential. Hence when comparing pBTTT with P3HT, the presence of the unsubstituted thieno[3,2-b]thiophene reduces the number density of alkyl attachments, and hence lowers the conjugated electron density. Additionally, the delocalization of electrons from the thienothiophene aromatic ring into the backbone is less favorable than from a thiophene ring, due to the larger resonance stabilization energy of the fused ring over a single thiophene ring. Hence, the higher energy quinoidal form is less favorable for thienothiophenes, and this reduced delocalization along the backbone, as well as the reduced inductive electron donation from the fewer alkyl chains per repeat unit, causes a lowering of the polymer HOMO energy level compared to P3HT. The pBTTT monomer units adopt an essentially coplanar conformation along the backbone, as illustrated in the cross-section of the conformational view along the long axis shown in Figure 3a, allowing neighboring polymer backbones to assemble in a closely packed, tilted face-to-face arrangement.[31,32] This creates an extended order microstructure (so called π-stacked lamella) facilitated by the planarity of the monomers. Both monomers are centrosymmetric, and the polymer repeat unit has a rotational symmetry. The optimal backbone conformation has an all ''anti'' sulfur arrangement across the short axis, as illustrated in Figure 1c, facilitating main chain extension as a stiff ''rigid rod'' shape, alternately bending to accommodate the non-linear bond angle between adjacent thiophene units. This both extends the longer range linearity of the backbone and helps facilitate both backbone π stacking and side chain packing and interdigitation between stacked lamella, shown in Figure 3b, leading to a highly ordered and laterally extended microstructures composed of π-stacked lamella, registered in the third dimension by the side chains.

4.3. pATxT

Poly(3,6-dialkylthieno[3,2-b]thiophene-co-bithiophene) **5** (pATBT) polymers shown in Figure 1d have the same backbone molecular skeleton as pBTTT, with a fully delocalized π electron system, but differ in the attachment location of the side chains, which in this case project from the 3rd and 6th positions of the thieno[3,2-b]thiophene monomer. It has been experimentally measured that the HOMO energy level of pATBT polymers is about 0.05–0.1 eV lower lying than pBTTT. This may be due to the possible rotational torsion of the thiophene rings of the bithiophene unit[33] leading to reduced π orbital overlap, or possibly the reduced impact of the electron donating alkyl groups into the more resonantly stabilized thienothiophene. However, the monothiophene polymer analogue (pATMT) was measured to have a similar HOMO energy level to pATBT, and did not have this torsional feature, and also has a greater ratio of electron donating alkyl chains per repeat unit. The alkyl side chain spacing distance for the pATBT polymer series is both regular and large enough to facilitate interdigitation. As both side chains are coupled to the same unit, any ring movement will require the cooperative motion of both alkyl chains, which may hinder the formation of the optimal coplanar conformation on crystallization. Conversely, once assembled, it may be more stable to perturbations. Copolymers of the dialkylthienothiophene monomer with both unsubstituted thieno[3,2-b]thiophene **6** (pATTT)[34] and thieno[2,3-b]thiophene **7** (pATCT) have also been reported. In contrast to thiophene containing polymers, where the angle formed from the projection of the bonds that link a thiophene monomer at the 2nd and 5th positions is less than 180°, the 2,5-thienothiophene link gives rise to polymers with a fully linear backbone. Rotation of the thiophene ring in the backbone is a cooperative motion requiring rotation of neighboring thiophene units, (nonrotationally invariant) due to the nonlinear linkage,

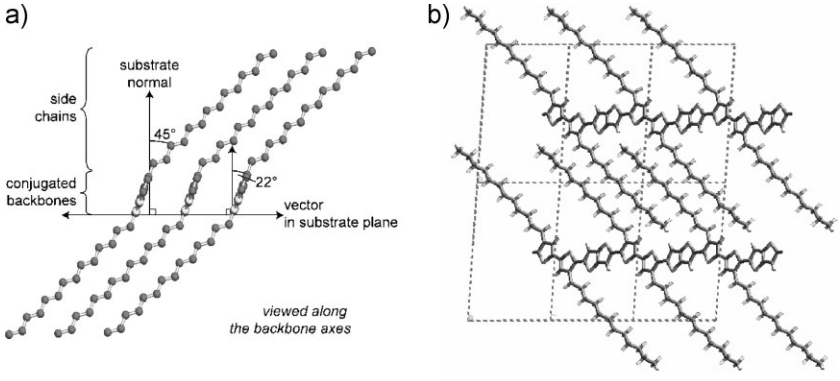

Figure 3. a) Cross-sectional view of pBTTT backbone conformation, illustrating coplanarity of the backbone, backbone tilt with respect to lamella plane, and extended, ordered side chains. Reproduced with permission from [31]. Copyright 2007 Wiley. (b) Front view of pBTTT backbone, illustrating the ''anti'' arrangement of adjacent sulphur atoms along the backbone and side chain interdigitation (courtesy of Patrick Brocorens Université de Mons-Hainaut, Belgium).

whereas the linear thienothiophene is rotationally invariant. The impact of this difference on the all-thienothiophene polymers is still being evaluated.

5. Polymer Structure Optimization

In order to achieve highly crystalline thin films consisting of closely packed conjugated backbones, polymer design requirements focus on aromatic-coupled monomers with low polar functionality, which form stiff, planar conformations. Consequently high melting temperatures are exhibited, and polymer solubility is very poor in most organic solvents. Increasing the alkyl side-chain fraction of the polymer through extending the chain length or increasing the degree of substitution, typically can be used as a tool to improve solubility, as can introducing polar or bulky functional groups to either the side chains or backbone. The latter strategy for solubility enhancement is often achieved, however, at the expense of disrupting the close-packed morphology required for optimum charge transport.[35] The inclusion of an electron-withdrawing ester group as a substituent in the 3rd position on the thiophene monomer was previously demonstrated in thiophene polymers.[36] The ester groups served to both further solubilize the polymer and increase the ionization potential in comparison to the simple alkyl chain substituent analogues, without disrupting the closely packed and crystalline morphology. In this approach, a mobility of 0.06 $cm^2 V^{-1} s^{-1}$ was achieved in comparison to a mobility of 0.12 $cm^2 V^{-1} s^{-1}$ for the analogous alkyl derivative.[33] This approach was utilized to prepare an analogue of pBTTT, shown as polymer **2** in Table 1. The resulting polymer was amorphous, with no thermal transitions observable by differential scanning calorimetry (DSC). The mobility dropped by over one order of magnitude to 0.01 $cm^2 V^{-1} s^{-1}$ most likely due to the loss of order, however, the polymers exhibited improved ambient operational stability.

Polymer molecular weight[28–34] and polydispersity also have a strong influence on thin-film microstructure and thermal behavior.[37–43] Low molecular weight pBTTT-C_{12} ($M_n = 8$ kDa) was observed by atomic force microscopy (AFM) measurements as shown in Figure 4a [18] to have a highly crystalline, rodlike, whisker or hay-stack microstructure. This is similar to that observed for low molecular weight P3HT. It is believed that each rodlike domain comprises face-stacked polymer chains, the width corresponding to the length of each polymer chain, and the length of the rod corresponding to the number of stacked chains. DSC experiments reveal that there is only one thermal transition, occurring at about 170 °C, shown as the inset in Figure 4a. As the molecular weight increases to 12 kDa, the domains become more nodular and better connected, as shown in Figure 4b, the backbone melt temperature rises to about 185 °C (inset in Figure 4b, and there is now evidence of an additional small endotherm at lower temperature, indicating that the polymer exhibits a small liquid crystalline phase. Higher molecular weight polymer ($M_n = 30$ kDa) exhibits a more three-dimensional microstructure with larger crystalline domains, as shown in Figure 4c, and there are now two clear melting transitions observed with DSC, indicating a broad mesophase between 150 °C and main chain melt at about 250 °C. The low molecular weight films typically exhibit almost an order of magnitude lower mobilities, as shown in Figure 4d. This relationship has also been observed for P3HT polymers, and several explanations have been proposed. It appears that the higher molecular weight P3HT has more aligned and connected grains, whereas the low molecular weight P3HT has more pronounced grain boundaries.[38] An enhanced out-of-plane backbone conformation twisting in low molecular weight polymer has also been proposed as an explanation for the difference in mobility.[39] This deviation from planarity decreases the effective conjugation length and reduces the efficiency of charge hopping. A study in the high mobility regime has correlated increase in the molecular weight with increasing crystalline quality within domains, with fewer chain ends per domain or ''nanoribbon'' as well as the possibility for individual polymer chains to bridge between domains at high molecular weight.[42] However, at high molecular weights ($M_n > \sim 50$ kDa) there is an increase in crystalline disorder, possibly due to slower crystallization kinetics from higher viscosity. It was also observed that charged polaron delocalisation is significantly larger as the molecular weight increases.

6. Thermal Behavior

The three series of thienothiophene polymers, when appropriately substituted or copolymerized with suitable co-monomers, can exhibit extended planar backbone conformations, facilitating closely packed π stacked crystalline lamella like microstructures. Attaching the side chains in such a way that they have optimal spacing and are not sterically prevented from ordering, allows them to pack and interdigitate into organized domains. On heating, thienothiophene polymers with organized side chains can exhibit a thermotropic liquid crystalline phase which originates as a consequence of side chain melting. Both pBTTT and pATBT polymers exhibit a side chain melt at all side chain lengths that were synthesized (from C_{12}–C_{18}), however pBTCT polymers do not, possibly due to a lack of chain order due to the irregular spacing distances. On heating the liquid crystalline polymers above the side chain melt, the mesophase persists until a main chain melting thermal transition occurs. We have recently extensively characterized the structure of the mesophase of pBTTT-C_{14} in the 120–180 °C temperature range.[31] We found that very high layer quality was achieved upon entry into mesophase indicating smectic-like order. Additionally, the level of side chain gauche defects achieved a plateau within the mesophase, confirming that the transition involves the melting of the interdigitated side chains. The melt transitions, and their subsequent crystallizations on cooling can be clearly determined from the DSC data shown for all three polymer series in Figure 5a–c. There is some evidence of anisotropy in pBTTT polymers on heating above the backbone melt temperature, and even that this anisotropy increases with time held above the melt. This is currently being investigated. The melting temperature of the pBTCT polymers, of equivalent side chain length, is lowest at comparative chain lengths, as illustrated in Figure 5d, probably due to the less linear backbone conformation and irregular side-chain spacing, with the pATBT exhibiting the highest melting temperatures. Increase in the alkyl chain length within the same polymer backbone series, typically had the most effect on the first melting transition, but also slightly

Table 1. Properties of Thienothiophene Containing Polymers.

Polymer	Comonomer	Comonomer	HOMO Energy Level [a]	Saturated Charge Carrier Mobility [$cm^2\ V^{-1}\ s^{-1}$]
1[30]	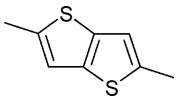	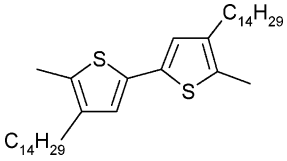	5.05	0.63
2[66]	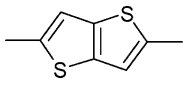	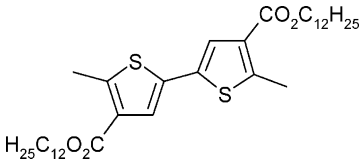	5.25	0.01
3[67](see also [56] for C_9H_{19})	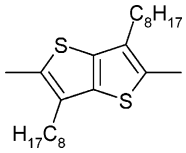	–	n.a.	1×10^{-6}
4[68]	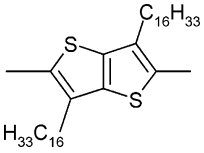	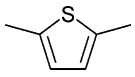	5.00	0.30
5[68](see also [69] for $C_{15}H_{31}$ and [34] for C_9H_{19}))	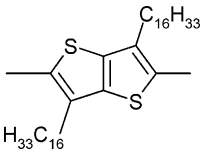	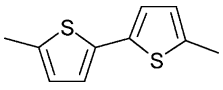	5.1	0.20
6[68,70] (see also [34] for C_9H_{19})	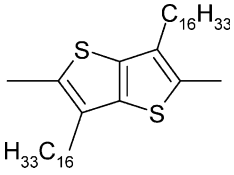	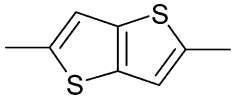	5.25	0.02
7[68]	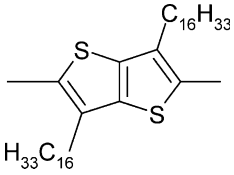	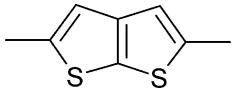	5.4	0.007
8[26]	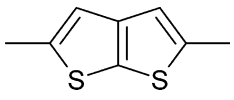	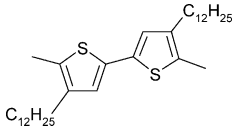	5.3	0.03
9[71]	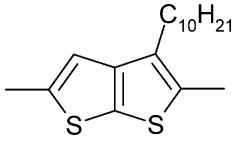	–	n.a.	3×10^{-5}
10[56]	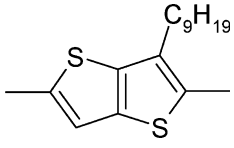	–	n.a.	n.a.

[a] Determined by an ambient photoelectron spectroscopy method with a Riken-Keiki AC-2 Spectrometer.

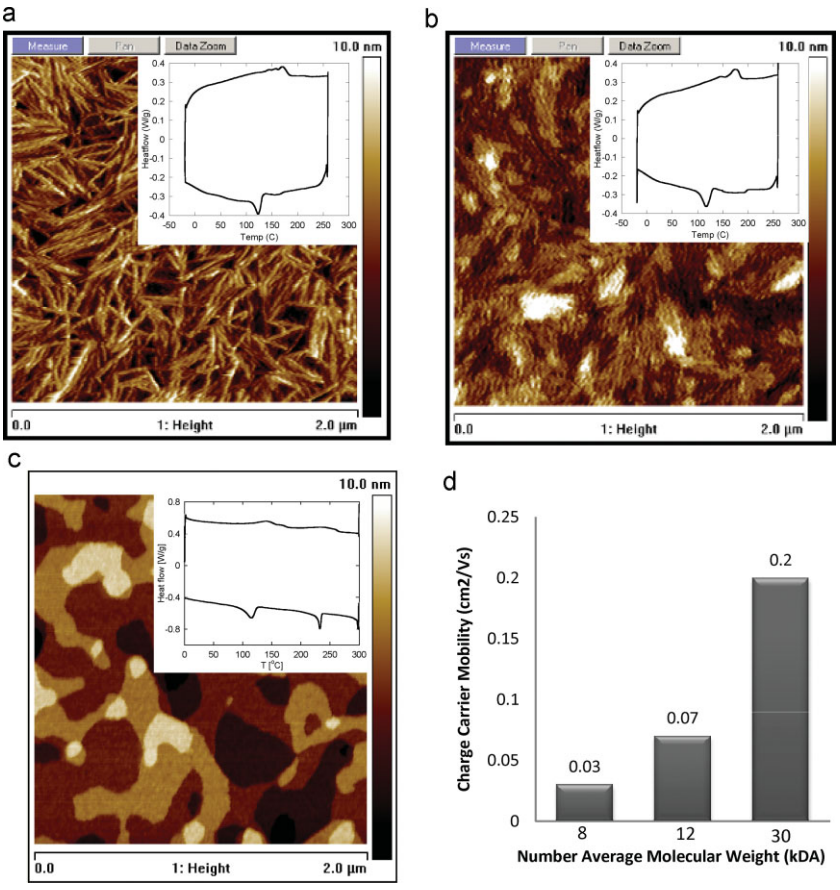

Figure 4. AFM images of pBTTT films with molecular weight of a) 8 kDa, b) 12 kDa, and c) 30 kDa. d) Plot of field effect mobility as a function of molecular weight. Inset of (a-c) are DSC plots showing the phase transitions.

reduced the main chain melt. Relatively high melting enthalpies are observed for these crystalline polymers, suggesting a high level of crystallinity of both side and main chains, consistent with the model of an interdigitated, closely packed polymer conformation. Interestingly, analogues of the pATBT polymers, where the bithiophene monomer is replaced with monothiophene (pATMT) **4**, has a consistently lower melting point by about 40 °C for all side chain lengths synthesized. The inclusion of unsubstituted thieno[3,2-b]thiophene (pATTT) **6**, or unsubstituted thieno[2,3-b]thiophene (pATCT) **7** as a copolymer unit, affords a linear backbone, and this has a significant effect on the thermal behavior. Although, low temperature endotherms are observed by DSC, which we ascribe to side chain melting, they do not appear to exhibit a main chain melt, perhaps due to a stiffer backbone. The homopolymers of monoalkylthienothiophenes **9** and **10** also have a linear backbone and do not show a main chain melt.

7. Thin Film Microstructures

Optimum semiconductor charge carrier mobilities were achieved by promotion of thin film microstructures comprising large crystalline domains where the π-stacked lamella assemble in the plane of the device substrate, i.e., in the plane of the accumulation layer formed at the semiconductor-dielectric interface between the source and drain electrodes. This "edge-on" backbone orientation can be created by either pre-aggregation of the lamella into platelet-like domains or by applying a low surface energy self-assembled monolayer (SAM) such as hexamethyldisilazane (HMDS) to the substrate surface.[44,45] Introduction of an annealing step at a temperature within the mesophase, which further promotes this orientation and significantly allows the growth of highly ordered crystalline domains. The coalescence of domains is facilitated by the low mesophase viscosity and good inter-grain connectivity which is promoted from domains being co-aligned by the low energy surface. Domain growth is additionally favored by the interdigitation of the side chains. A range of experimental techniques were used to elucidate the details of this microstructure and are discussed in the following sections.

7.1. X-Ray Scattering

We have extensively examined the ordering of these thienothiophene polymers in thin films using X-ray scattering.[30,46,47] These studies helped to reveal the molecular ordering in the crystalline domains as well as the orientation of these domains relative to the direction of electrical transport. We have used a combination of two-dimensional imaging of the X-ray scattering at grazing incidence and higher resolution measurements at specular and grazing incidence to provide a detailed understanding of these features. Although, the backbone structures of pBTCT, pBTTT, and pATBT are similar, their differences cause significant changes in their molecular ordering.

The basic packing structure of the poly(alkylthiophene-thienothiophenes) is similar to that of the poly(alkylthiophenes) with important differences.[48] The structure of pBTTT provides a good basis for understanding the basic features of these materials (Fig. 3). Like poly(3-hexylthiophene) (P3HT), the conjugated backbones of pBTTT are π-stacked into two-dimensional "sheets"; these sheets are separated into lamella by the alkyl sidechains.[20] Unlike P3HT, due to the spacing between the sidechains along the repeat unit of pBTTT, they are free to interdigitate as we discuss more extensively in a later section.[25] The crystalline domains in as-cast films of pBTTT are textured with the lamellar stacking direction along the surface normal. The texturing is imperfect as significant arcing of the diffraction peaks is observed.[32] The ordering of the films can be improved by thermal annealing into the liquid crystalline phase (near 140 °C) followed by cooling to room temperature. After this process higher index peaks are observed indicating the formation of three-dimensionally ordered domains (Fig. 6b). The interdigitation of the sidechains is important for registry of the polymer

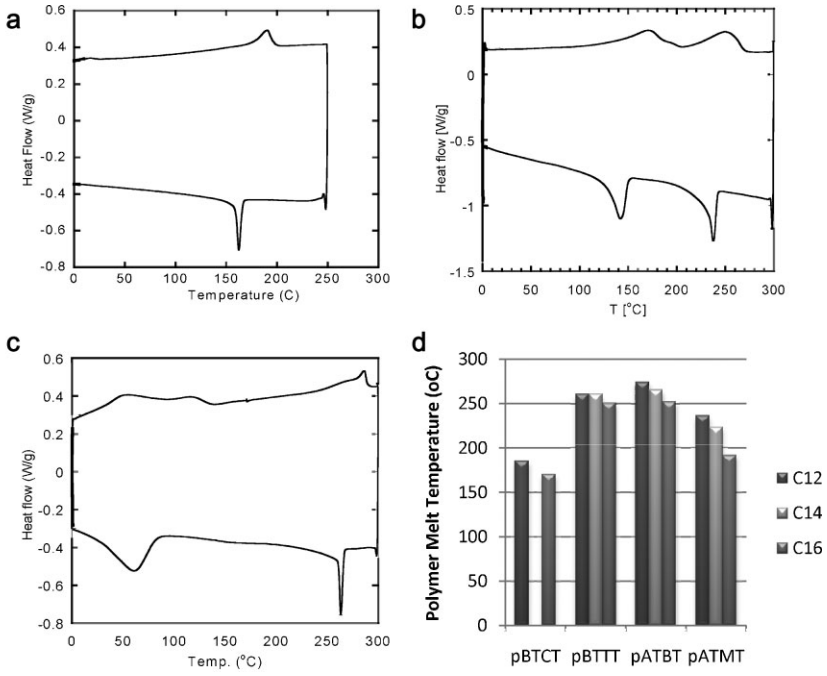

Figure 5. DSC plots showing second scan heating (endo up) and cooling curves at 10 °C min^{-1} of a) pBTCT-C_{10}, b) pBTTT-C_{10}, and c) pADBT-C_{14}. as well as d) the side chain dependence on melting temperature of thienothiophene polymer series pBTCT, pBTTT, pATBT, and pATMT.

chains because it helps to lock in the positional ordering along the polymer backbone. Interestingly, the lamellar spacing may increase or decrease after annealing by 1 to 2 Å. This change is relatively small and can be accomplished by small conformational changes of the alkyl sidechains. Measurement of the X-ray scattering as a function of temperature shows a dramatic change in the lamellar spacing at the LC transition indicating that the as-cast film has a metastable structure that is reordered in LC mesophase. This metastable structure is likely due to the relatively fast drying time of spin-coated films that prevents the molecules from reaching their most stable structure.

Despite the difference in the fused thienothiophene ring between pBTCT and pBTTT, they exhibit similar X-ray scattering peaks. The lamellar spacing observed along the specular direction is 18.4 Å for pBTCT-C_{12} and is 19.2 Å for pBTTT-C_{12} and the in-plane spacings are nearly identical ($q_{xy} = 1.41$, 1.70, and 1.90 $Å^{-1}$). Annealed films show larger differences as the scattering pattern for annealed films of pBTTT comprise multiple high index peaks that are not observed for pBTCT. Additionally, there is significant arcing of the peaks for pBTCT even in annealed films indicating that the crystalline domains are misoriented relative to the surface normal. The backbone of pBTCT is not likely to be as linear as that of pBTTT due to the energetic preference of an "anti" configuration of adjacent sulfur atoms in the heterocycles, which may interfere with the ordering even after annealing.

While pBTTT and pATBT share the same backbone structure, they have substantially different X-ray scattering patterns. The lamellar spacing for pBTTT-C_{16} is 23.5 Å whereas that for pATBT-C_{16} is 21.6 Å. The in-plane feature of pBTTT at $q_{xy} = 1.69$ $Å^{-1}$ (d-spacing of 3.71 Å is not observed for pATBT, but a feature at ~1.57 $Å^{-1}$(d-spacing of 4.0 Å) is present. Typically features near spacings of 3.8 Å are assigned as the π-stacking distance. Although this shift may appear striking, this peak does not necessarily represent the separation of the polymer chains. Our modeling efforts for pBTTT suggest the unit cell is triclinic and that this peak is actually (110) peak rather than (010) as suggested in our initial publication.[49] It is possible that pATBT does not have an orthorhombic cell and that this peak is not the π-stacking distance. Detailed modeling is required before the unambiguous assignment of X-ray scattering peaks to molecular packing features can be achieved. Both of these polymers, however, do show higher order peaks and highly oriented textures suggesting that the placement of the alkyl side chains along this basic repeat unit is not as significant of a perturbation as incorporation of a thieno[2,3-b]thiophene monomer, as in pBTCT.

7.2. NEXAFS

The thienothiophene polymers are complex macromolecules with significant conformational freedom. Polarized photon absorption spectroscopies provide a means to probe the orientational order of the various chemical moieties of which the thienothiophene polymer is composed. Near-edge X-ray absorption fine structure (NEXAFS) spectroscopy[50] is particularly sensitive to the orientation of the conjugated planes and side chains of organic semiconductors, and can be used to probe these aspects of orientation in thienothiophene polymers.

NEXAFS spectroscopy is sensitive to the absorption of soft X-rays into resonant excitations of core, typically 1 s, electrons to unfilled, typically antibonding, molecular orbitals. The technique therefore provides elemental composition information by the core shell that is accessed, which dictates the energy range of

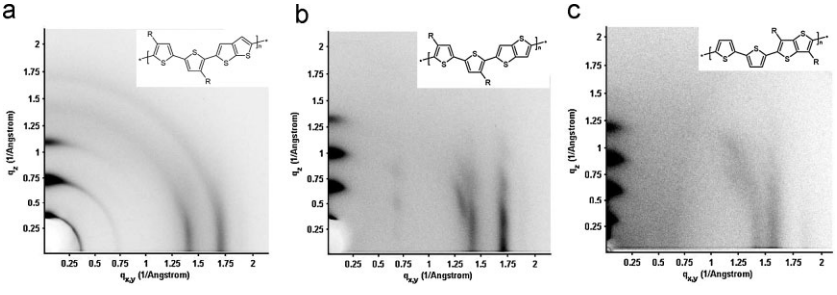

Figure 6. Two-dimensional images of the X-ray scattering at grazing incidence of thin films of a) pBTCT-C_{12}, b) pBTTTT-C_{12}, and c) pATBT-C_{16} after annealing in the liquid crystalline mesophase. The data are given as a function of the scattering vector q, where $q = 2\pi/d$.

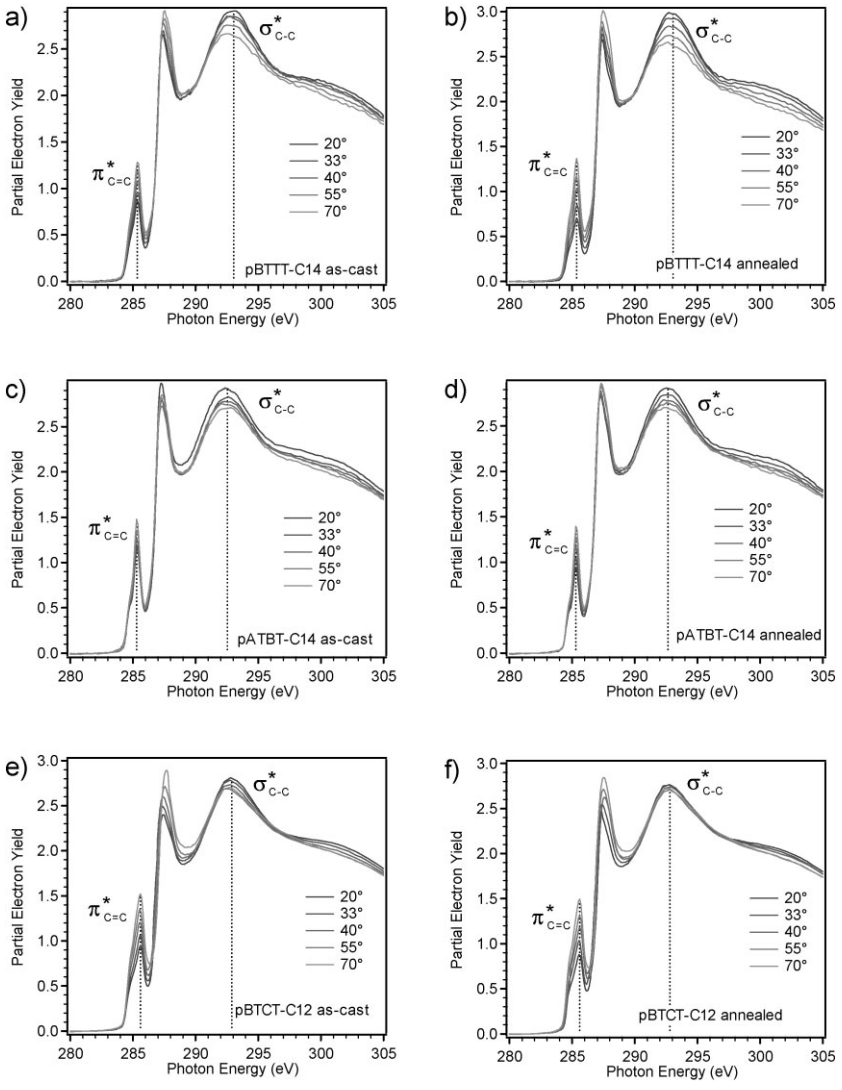

Figure 7. NEXAFS spectra collected at several incident angles per sample. a,b) pBTTT-C_{14} films as-cast, and annealed, respectively. c,d) pATBT-C_{14} films as-cast, and annealed, respectively. e,f) pBTCT-C_{12} films as-cast, and annealed, respectively. Standard uncertainty of the partial electron yield is ±2%.

the spectroscopic scan, and also provides molecular structure information by the shapes and intensities of the resonances within the spectra. Orientation information is typically collected by changing the angle of the sample with respect to the incident beam in a manner that adjusts the angle between the electric field of the polarized beam and the sample normal. The resonance orientation will depend on the overlap between the electric field vector and the resonance orientation. The resonance orientations for typical NEXAFS excitations are straightforward to describe; a 1 s → σ^* excitation will be oriented parallel to the σ bond, while a 1 s → π^* excitation will be orientation perpendicular to the π bond (in both cases approximately along the vector described from the center of the bond to the greatest electron density in the final state orbital). A rigid aromatic ring, or coplanar system of conjugated aromatic rings, will exhibit a single, summed π^* resonance orientation perpendicular to the ring plane.

NEXAFS spectra of three thienothiophene polymers are shown in Figure 7. Prominent resonances common to all three polymers are the carbon-carbon 1 s → π^* transition near 285 eV, the carbon-hydrogen 1 s → σ^* transition near 288 eV (overlapping with Rydberg transitions and the step edge), and the carbon–carbon 1 s → π^* transition near 293 eV. The π^* transition can be assigned to the conjugated planes of the thiophene and thienothiophene rings of the polymer backbone. We note that all of the spectra show some additional structure in the π^* resonance, most notably a lower-energy shoulder below 285 eV; these additional resonances reveal populations of inequivalent carbon–carbon double bond lengths, consistent with the molecular structures of the polymer backbones. While this fine structure is almost identical for pBTTT and pATBT, there are some differences between those π^* spectra and that of pBTCT, particularly a more intense lower-energy peak in pBTCT, consistent with the different backbone structure of pBTCT. The carbon–carbon σ^* transition contains some contribution from the backbones, but its intensity is dominated by resonances of the alkane side chains; the location and shape of the resonance is therefore nearly identical for all three materials.

The orientation of the conjugated planes of the three polymer semiconductors can be determined by the variation in π^* intensity with changes in incident angle. For all three materials, the π^* resonance is most intense when the beam is nearly perpendicular to the sample (e.g., when the electric field vector is nearly parallel to the sample). This dependence indicates that the π^* resonance is oriented preferentially parallel to the substrate plane. Because the π^* resonance of an aromatic ring or coplanar aromatic ring system is perpendicular to the ring plane, this dependence indicates that the backbone plane must be preferentially ''edge-on'' upon the substrate.

The degree of orientation preference can be quantified by a dichroic ratio, R, which can vary from +0.7 for a perfectly edge-on conjugated plane to −1.0 for a perfectly flat or ''plane-on'' conjugated plane (graphene, for example). We quantify the orientations of the thienothiophene polymer conjugated planes in Table 2. All are positive, reflecting the preferentially edge-on plane tilt in all cases. In pBTTT and pATBT, the conjugated plane orientation becomes more vertical after thermal processing. In pBTCT, thermal processing has no effect, consistent with its lack of a significant thermal transition in DSC below the primary backbone melt. The annealed pBTTT-C_{14} exhibits the most edge-on conjugated plane of the three materials, but the orientation is quite similar to that of the other two materials. The less positive dichroic ratios in pATBT-C16 and pBTCT can be

Table 2. Polythienothiophene conjugated plane orientations

	π^* Dichroic Ratio R	
Material	As-cast	Annealed
pBTTT-C_{14}	0.27 ± 0.01	0.41 ± 0.01
pATBT-C_{14}	0.13 ± 0.04	0.21 ± 0.01
pBTCT-C_{12}	0.31 ± 0.01	0.33 ± 0.02

explained either by a less vertical preferential plane tilt or some extent of disorder in the film.

In the case of pBTTT, we have shown by complementary measurements including AFM and spectroscopic ellipsometry that the amount of noncrystalline material in the films is ≈7% or less.[31] It is then reasonable to assume that the orientation distribution of the conjugated planes of pBTTT is narrow and monomodal, and assign a specific angular tilt to the conjugated plane. This tilt is ≈22° from the perfect edge-on case for pBTTT. We have shown that this conjugated plane tilt is predicted by density functional theory calculations; in fact, it is predicted to occur in many thiophene polymers.[51] If we were to make the same assumption for heat-treated pATBT and pBTCT, we would arrive at tilts of 28° and 25°, respectively, but the assumption and tilt assignment cannot be made with confidence without complementary information regarding likely orientation distributions.

The orientations of the side chains can be determined from the dichroism of the σ^* resonances, after subtraction of the step edge from the resonance intensity, and compensation for the contributions from the backbones, which are nominally parallel to the substrate. The side chains of pBTTT tilt by ≈45° from substrate normal by this analysis. With a narrow orientation distribution, the side chain tilts for pATBT and pBTCT would be ≈50° and ≈55°, respectively. We note that the orientation of the pBTCT side chains is very close to the ''magic angle'' orientation, and therefore is equally consistent with disordered side chains in the absence of additional side chain conformation or orientation distribution information.

7.3. AFM

AFM imaging provides a measure of the surface topography. As cast films of pBTTT and pBTCT look similar to typical P3HT films with an isotropic nodule-like structure. Annealing the films above the liquid crystal transition transforms the structure into an ordered structure with substantially larger domains, as shown in Figure 8a and b, that correlate with an increase in the charge carrier mobility. pBTTT films form large molecular terraces[31,25,45] where the molecular step corresponds to the lamellar spacing measured by XRD. These terraces have domain sizes of several hundred nanometres and are a direct visualization of the π-stacked lamella structure inferred from the XRD results for polythiophenes. Transmission electron microscopy on pBTTT-C_{14} films annealed on a substrate treated with OTS and delaminated revealed that the terraces might comprise subdomains that are approximately ~10 nm wide.[51b] pBTCT films form rounded ≈50 nm domains. The smaller domain size and the rounded shape are likely a result of the fact that the pBTCT polymer conformation has a crank shaft shape. The pBTTT monomer, on the other hand, has a more regular shape and forms large, extended domains. pATBT has a moderately ordered structure with weak terracing as shown in Figure 8c. The domains are considerably smaller than the domains observed for pBTTT. The reduced ordering is consistent with the other structural measurements.

7.4. Interdigitation

The detailed packing behavior of thienothiophene polymers can be revealed by a strategy that combines diffraction techniques, which determine the spacings of regular molecular order, and linear polarization spectroscopies, which determine the substrate-relative orientations of molecular moieties. When this strategy is applied to thienothiophene polymers, a signature packing motif of interdigitated side chains can be revealed.[31] Diffraction of pBTTT-C_{14} reveals a layer d-spacing of 2.1 nm. Spectroscopic orientation measurements of the side chains by both FTIR and NEXAFS indicate that the side chains tilt ≈45° away from surface normal. Importantly, complementary methods such as spectroscopic ellipsometry show that the amount of noncrystalline material in the films is extremely small, enabling the key assumption that the orientation distribution of the side chains is tight and monomodal. This assumption is further justified by FTIR measurements of side chain conformation by the energetic location of the methylene group antisymmetric stretch; the stretch position in pBTTT is consistent with nearly all-*trans* alkane chains. Given the ≈45° tilt of the side chains, and the backbone layer spacing of 2.1 nm, the side chains of vertically adjacent backbones are required to substantially interdigitate.

A simple model can evaluate the feasibility of side chain interdigitation in thiophene polymer systems where the π-stacking distance and side chain attachment points along the backbone are known.[25] The side chains may be regarded as attached in a fixed planar density dictated by the p-stacking distance and the side-chain-attachment repeat distance (analogous to a fixed graft density on a planar substrate). The density of the alkane chains in their closest-packed plane is a simple

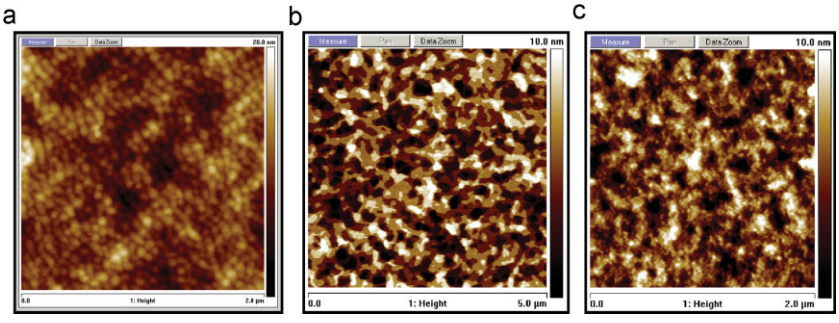

Figure 8. AFM images of a) pBTCT film annealed at 180 °C on an OTS treated substrate, b) pBTTT, film annealed at 180 °C on an OTS treated substrate, and c) pATBT film annealed at 120 °C for 5 min on an OTS substrate.

function of their attachment density, the substrate-relative alkane chain tilt, and whether the side chains are interdigated (which doubles the density). Comparison of the density of the alkane chains in their closest-packed plane to the methylene density in crystalline polyethylene can be used to evaluate the feasibility of interdigitation. This analysis shows that the side chains of pBTTT will achieve a polyethylene-like density when they are tilted at 45° with respect to surface normal and interdigitation, consistent with our experimental finding. This model also predicts that the side chains of pATBT and pBTCT are capable of interdigitation. The similar chain tilt and lamellar repeat observed for pATBT, together with preliminary IR and ellipsometry results, confirm interdigitation for that series. We cannot currently confirm the case for pBTCT. Importantly, this model also shows that the side chains of P3AT's cannot interdigitate (at least for the most common π-stacking distance of P3AT's) because they are too densely attached long the backbone. This key difference between pBTTT and P3HT may explain the greater three-dimensional order seen in pBTTT; side chain interdigitation provides a mechanism for three-dimensional molecular registry. The simple model provides a framework for predicting whether a given primary chemical structure is capable of interdigitation. The melting of the crystalline, interdigitated side chains provides a mechanism for ''repairing'' defects in as-cast films by access to the smectic-like mesophase where the side chain constraints are minimal and the backbones have sufficient molecular diffusivity to rearrange into large, well-ordered domains. The high levels of layer order and domain size are locked-in upon cooling by the interdigitation and crystallization of the side chains.

8. Transistor Properties

The p-type charge carrier mobility of thienothiophene polymers was routinely determined in bottom-contact, bottom-gate field-effect transistor devices (measurement details are provided in the General Experimental Methods section). This device architecture is convenient as the semiconductor is only exposed to one thermal processing step, and high quality, readily available patterned substrates can be prepared separately. The technique was therefore developed as a routine screening method. The saturation regime mobility μ_{SAT} was calculated from the saturation regime transfer characteristics using the equation:

$$I_D = \frac{WC_i}{2L}\mu_{SAT}[V_0 - V_G]^2 \quad (1)$$

where W is the transistor channel width, L the channel length, V_0 the turn-on voltage, V_g the gate voltage, and μ_{SAT} was derived from the slope of a plot of $(I_D)^{1/2}$ versus V_G.

The charge carrier mobility values of a range of thienothiophene polymers have been measured and are collected in Table 1. In several cases values approach that of high performing, evaporated small molecule devices[52] and are comparable to amorphous silicon. In general, mobilities were measured to be higher in inert atmosphere than ambient, perhaps due to the presence of charge transfer complexes due to atmospheric impurities, which may act as traps. Unless explicitly stated, the values reported were measured in nitrogen. Charge carrier mobilities of about 0.03 $cm^2\ V^{-1}\ s^{-1}$ can be achieved by pBTCT polymers, at standard channel lengths of 10–20 μm, with corresponding ON/OFF ratios around 10^6 in air. Higher charge carrier mobilities of up to 0.1 $cm^2\ V^{-1}\ s^{-1}$ were observed for shorter channel lengths of 5 μm. The linearity of the output characteristics at low source-drain voltages suggest that even with the lower HOMO energy level, good charge injection from gold electrodes is still possible. PBTTT polymers generally exhibited the highest mobilities of all thienothiophene polymers measured, with values of up to 0.6 $cm^2\ V^{-1}\ s^{-1}$ obtained at a 20 μm channel length for polymers with a C_{14} side chain length. In contrast to reported values for P3HT transistor devices,[53–55] there is less than a factor of two difference in charge carrier mobility for pBTTT polymers on varying the alkyl chain length from C_{10} to C_{18}, with a maximum mobility observed at a chain length of C_{14}. Charge carrier mobilities of up to 0.2 $cm^2\ V^{-1}\ s^{-1}$ were measured for pATBT polymers in both air and nitrogen, demonstrating the stability of this polymer class. The monothiophene copolymer (pATMT) also exhibited high charge carrier mobility, in this case up to 0.3 $cm^2\ V^{-1}\ s^{-1}$ in a dry nitrogen atmosphere. This analogue however was not as stable in ambient as the bithiophene polymer even though the HOMO energy levels were measured to be similar. Mobilities of 0.02 and 0.007 $cm^2\ V^{-1}\ s^{-1}$ for copolymers of dialkylthienothiophene with thieno[3,2-b]thiophene analogue **6**, and thieno[2,3-b]thiophene analogue **7** were obtained, respectively.

A regioregular homo polymer of 3-nonylthieno[3,2-b]thiophene was also prepared (Table 1, **10**); however, the molecular weight and solubility was low.[56] Charge transport characteristics were not reported. The homo polymer of 3,6-dimethoxythieno[3,2-b]thiophene[57] and copolymers of 3,4-dialkoxythieno[2,3-b]thiophene[58] have recently been reported as a possible alternative to the conducting polymer ethylenedioxythiophene (PEDOT).

Copolymers of thieno[3,2-b]thiophene[59–61] and thieno[2,3-b]thiophene[62] with 9,9-dialkyl fluorene have also been reported for both transistor and OLED applications. In the case of the thieno[3,2-b]thiophene copolymer, the material exhibited thermotropic liquid crystalline behavior with a nematic phase at high temperature.[63] Field effect mobilities in p-type transistor devices were on the order of 10^{-3} $cm^2\ V^{-1}\ s^{-1}$. Although, the mobility value is on the low side of acceptable performance, a comparison to the well studied poly(9,9-dioctylfluorene-*alt*-bithiophene (F8T2)[64,65] under the same device conditions revealed slightly higher performance for the thieno[3,2-b]thiophene copolymer, demonstrating the potential for further optimization.

9. Low Contact Resistance Transistors

In order to probe the limits of carrier mobility in thienothiophene polymer devices, it is necessary to remove any barrier to charge injection at the contacts. The electronic properties of the polymer pBTTT-C_{14} were evaluated by fabricating organic thin-film transistors in a bottom-contact configuration using the high work function metal, platinum, as the contact electrodes (see the inset of Fig. 9a). The details of this fabrication process and mobility calculation are outlined in the General Experimental Methods section below. Figure 9a shows the transfer characteristics for a pBTTT-C_{14} device, operating in saturation. A mobility value of 1.1 $cm^2\ V^{-1}\ s^{-1}$ is extracted from the slope of the line

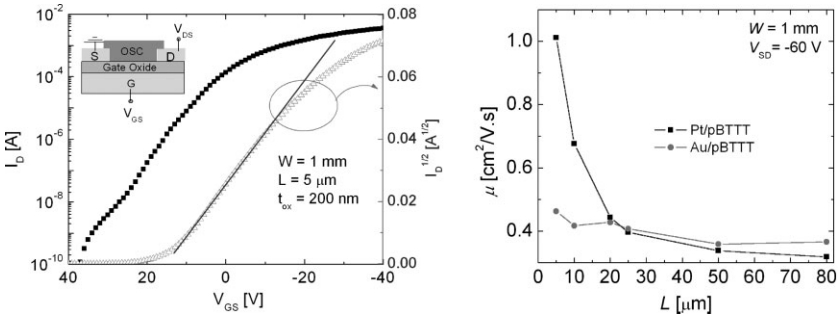

Figure 9. a) Transfer characteristics of a pBTTT-C_{14} transistor at room temperature and VDS = −60 V. From the slope of the line shown and the given device parameters, we extract a mobility of 1.1 $cm^2 V^{-1} s^{-1}$. Inset: Device cross section for a bottom-contact organic TFT. b) Plot of the saturation mobilities as a function of *L* for two sets of devices with different contact electrodes. Devices fabricated with Pt electrodes make better contact to pBTTT and the mobility shows a strong inverse *L* dependence.

shown in the plot, the highest mobility achieved to date for a solution-processed undoped polymer FET on an oxide insulator. At higher gate voltages, a deviation from this slope is observed in the data and has been attributed to the presence of contact effects. We find that optimization of device performance not only depends on the quality of the dielectric/semiconductor interface,[45,47] but also is dependent on the characteristics of the metal/semiconductor contacts. In particular, we have shown that large contact resistances between the metal and the organic semiconductor can reduce charge transport in the transistor channel.[21] Figure 9b shows a plot of the saturation mobility versus channel length for devices for devices made with Pt and Au electrodes. For the Pt devices, the mobilities increase as a function of decreasing *L*, reaching a maximum average of ~1 $cm^2 V^{-1} s^{-1}$ for 5 μm devices, while the calculated mobilities for the Au devices reveal only a small dependence on *L*.

As reported elsewhere,[72] this inverse *L* correlation with the saturation mobilities is most clearly observed in devices where the channel resistance is dominant over the resistance of the contacts. For the Pt devices, the contact resistances, even in short channel devices, are only a small fraction of the channel resistance whereas in the case of Au devices, the contact resistances are equal or larger than channel resistances for devices with $L \approx 15$ μm or less. In channel-dominated devices, more of the total drain voltage is dropped in the channel of the transistor, resulting in a higher effective electric field in the organic semiconductor. In disordered organic materials,[73] a higher longitudinal electric field can result in an increase in the mobility of the charge carriers according to the relation

$$\mu = \mu_0 \exp(\gamma\sqrt{E}) \quad (2)$$

where μ_0 is the zero-field mobility and the prefactor γ has been shown to depend inversely on *T*. In contact-limited devices, the longitudinal field in the channel is weak since a significant voltage is dropped across the contacts. This may mask the field-dependent mobility behavior.

10. Oxidative Stability

The fundamental thermodynamic electrochemical oxidation process of a neutral p-type semiconductor in ambient air under saturated humidity has been proposed to occur when the highest occupied molecular orbital (HOMO) energy level is less than 4.9 eV from the vacuum energy level.[74] It is therefore necessary to design the semiconductor such that the HOMO energy of the conjugated system (can also be referred to as increasing the ionization potential) is below this value, i.e., the ionization potential is greater than 4.9 eV.[29] Although the sensitivity to water and oxygen redox electrochemistry is not the only contributing factor to the instability of π-conjugated aromatics, it is necessary to ensure that the electrochemical oxidation of the semiconductor is not thermodynamically favorable. There are many reports in the literature that have observed instabilities in OFET performance in ambient air[29,75] and attributed this to an interaction with molecular oxygen.[24] For example, charge transfer complexes between thiophene and oxygen have been proposed, which can generate reversible charged states and a doping effect on transistor performance. It has been proposed that in the absence of light, oxygen is in fact not a strong oxidant for thiophene polymers, but instead that ozone, and possibly other pollutants in ambient air such as nitroxides, with high electron affinities are more likely to be responsible for doping.[76] This proposed explanation for semiconductor instability is consistent with recent evidence that top gate devices typically exhibit enhanced stability in comparison with bottom gate devices.[77] In this architecture, the semiconductor is protected from the environment by the dielectric and gate layers which may act as a sacrificial surface for reaction with highly reactive dopants such as ozone.

Conjugated thiophene polymers have electron-rich π-electron systems with relatively high energy HOMO levels rendering them susceptible to this process. Most design strategies to reduce the affinity of thiophene polymers to oxidative doping or degradation involve decrease in the HOMO energy level below the electrochemical oxidation threshold.[78] The HOMO energy level increases as the number of conjugated units along the backbone increases, up to a critical "effective" conjugation length, at which point it remains relatively constant. The conjugation length of the backbone can also be controlled by reducing the coplanarity and therefore π orbital overlap between adjacent thiophene rings or electronically by introducing a repeat unit into the backbone, which either inhibits or prevents delocalization. The HOMO energy level will also increase with increasing electron density of the conjugated system. Either including electron-withdrawing functionality within the conjugated system or reducing the density of electron donating functionality will contribute to lowering the energy. In the case of the thienothiophene polymers, all the approaches described above were employed to different extents, as described in the earlier Molecular Design section. The ionization potentials of all three polymers were measured by ultraviolet photoelectron spectroscopy (UPS) by the onset of the lowest binding energy signal, as shown previously in Figure 2. The cross-conjugated feature of the pBTCT polymer clearly manifests as a larger ionization potential (lower lying HOMO energy level) than either pBTTT or, pATBT, with the pBTTT

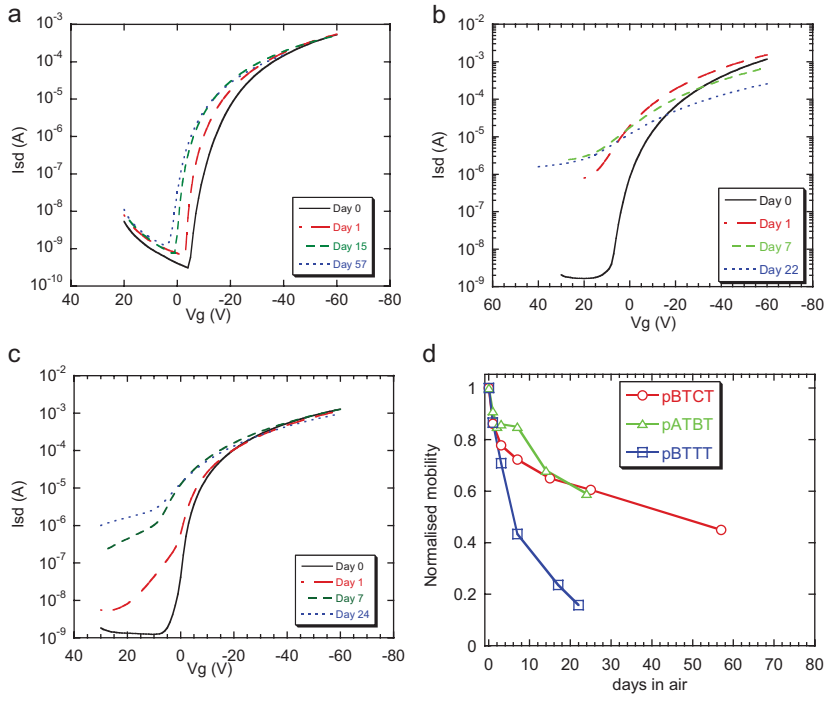

Figure 10. Ambient stability of FET devices. Transfer characteristics for polymer transistors with a) pBTCT; b) pBTTT and c), pATBT on prolonged exposure to air. d) Changes in normalized FET mobility calculated in saturation regime versus exposure time in air.

having the lowest ionization potential of the three polymers containing thienothiophene monomers.

The effect of thienothiophene polymer semiconductor exposure to ambient conditions over extended periods has been observed in the absence of light. Figure 10 describes the change in electrical characteristics of transistors fabricated with pBTCT, pBTTT, and pATBT semiconductors in a bottom-gate/bottom-contact configuration, in which the active semiconductor layer is the exposed top surface. Confirmation of significant oxidative doping in both the pBTTT and pATBT transistor device over continued ambient exposure time can be observed in Figure 10b and c as a rise in the transistor off-current, and a shift to more positive turn on voltage, due to an increase in acceptor states in the bandtail. The pBTCT polymer series showed the least evidence of oxidative doping, with only small changes in both OFF current and turn on voltage over almost two months exposure to air. Mobility values of both pBTCT and pATBT remained above 60% of their initial values for over 20 days, as shown in the comparative graph in Figure 10d. The difference in stability between pBTCT and pBTTT can clearly be attributed to the lower lying HOMO energy of pBTCT. However, the contrast between pBTTT and pATBT is remarkable considering the small difference in measured ionization potential.

Nevertheless, in filtered, low-humidity air, all transistor devices including pBTTT remained relatively stable over an extended period in the absence of light. Previous reports[30] have shown that the transfer characteristics of a pBTTT device recorded over a period of over 70 days show only a minor change in Off current and threshold voltage with a small decrease in On current. This corresponds to a drop in mobility over the measurement time-span by about a factor of three. Good stability has also been reported for repeated electrical stressing of pBTTT devices in ambient air over 50 h.[79] No special precautions were taken to exclude moisture in this case. These reported discrepancies suggests that the improvement in stability reported in low-humidity air may in fact be due to the unintentional removal of high electron affinity impurities such as ozone during the dehumidification process. The levels of such pollutants are likely to vary substantially from laboratory to laboratory, which is certainly experimentally observed.

11. Synthesis of Thienothiophene Polymers

11.1. Thienothiophene Monomer Preparation

Several routes have been developed to thieno[2,3-b]thiophene.[80–82] For example, Otsubu and co-workers reported an elegant synthesis by the lithiation of 1-trimethylsilylpentadiyne with n-BuLi/t-BuOK, followed by trapping of the resultant anion with carbon disulfide.[81] Ring closure upon work-up afforded 2-trimethylsilylthieno[2,3-b]thiophene, which could readily be desilylated by treatment with tetrabutylammonium fluoride to afford thieno[2,3-b]thiophene.[82] For larger scale preparations, a more convenient route was developed from commercially available 2-thiophenethiol (Scheme 1).[83] Thus alkylation with bromoacetaldehyde dimethyl acetal under Williamson ether conditions proceeded quantitatively to afford the protected aldehyde. Subsequent deprotection and ring closure occurred in one pot in the presence of polyphosphoric acid in refluxing chlorobenzene, to afford the product as a colorless oil.

Thieno[3,2-b]thiophene can also be prepared by a similar methodology, although 3-thiophenethiol is not commercially available and its preparation typically involves cryrogenic temperatures and organometallic reagents.[84,85] Several other routes to thieno[3,2-b]thiophene have been reported that are more readily amenable to scale-up.[80,86,87] For example 3-bromothiophene can be lithiated in the 2-position with a bulky non-nucleophillic base such as lithium diisopropylamine (Scheme 1). Quenching of the resulting thiophene anion with dimethylformamide or N-formylpiperidine afforded the thiophene aldehyde. Treatment of this *o*-bromoaldehyde with ethyl 2-sulfanylacetate in the presence of base afforded thieno[3,2-b]thiophene-2-carboxylic acid ethyl ester in high yield. Saponification of the ester group, followed by thermal decarboxylation of the resulting acid with metallic copper in refluxing quinoline afforded the unsubstituted thieno[3,2-b]thiophene in overall yields of roughly 60% over the four steps.[87]

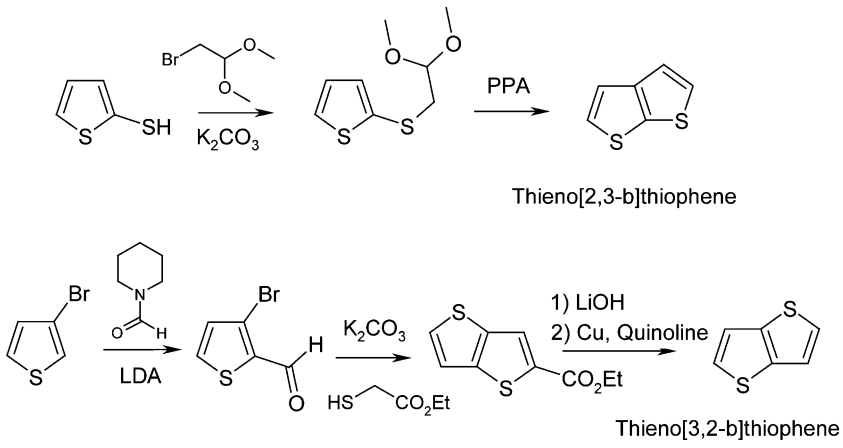

Scheme 1. Synthesis of thieno[2,3-b]thiophene and thieno[3,2-b]thiophene.

The synthesis of 3,6-dialkylthieno[3,2-b]thiophene has been reported by two alternate routes. Matzger and co-workers reported an elegant route starting from 3,4-dibromothiophene.[56] Acylation with decanoyl chloride in the presence of aluminum chloride afforded 2-decanoyl-3,4-dibromothiophene in good yield. Subsequent reaction with ethyl 2-sulfanylacetate under basic conditions afforded the mono-alkylated thieno[3,2-b]thiophene intermediate, which following hydrolyzation and thermal decarboxylation afforded 3-bromo-6-nonylthieno[3,2-b]thiophene. The second alkyl chain was then introduced into the 3-position by cross-coupling of bromine groups with 1-nonyne under Sonogashira conditions. Hydrogenation of the triple bond afforded the 3,6-dialkylthieno[3,2-b]thiophene. Ong and co-workers later applied the same chemistry to the synthesis of 3,6-pentadecylthieno[3,2-b]thiophene.[69]

We developed an alternative synthesis from 2-thieno[3,2-b]thiophene-carboxylic acid, which is readily prepared as outlined in Scheme 1.[67,68] Treatment of this carboxylic acid with excess bromine in acetic acid affords tetrabromo thieno[3,2-b]thiophene, through a combination of bromo-decarboxylation and bromination of the unsubstituted aromatic positions (Scheme 2).[88] The tetrabromo derivative was reduced with zinc in acetic acid to afford 3,6-dibromothieno[3,2-b]thiophene. A variety of alkyl chains could be readily introduced by Negishi cross-coupling under microwave heating with an appropriate alkylzinc halide in the presence of a palladium catalyst.

11.2. Polymerization of thienothiophene polymers.

pBTCT was synthesized by a copolymerization approach using Stille cross-coupling (Scheme 3). The distannyl monomer was readily prepared by lithiation of thieno[2,3-b]thiophene with two equivalents of n-butyllithium, followed by quenching of the resulting dianion with trimethylstannyl chloride. Trimethyltin was chosen as the organometallic group despite its high toxicity because it afforded a highly crystalline product which could be readily purified. In contrast, the incorporation of less toxic tributyltin groups resulted in a high boiling point oil, which was difficult to purify. Attempted polymerization led to low molecular weight polymers, most likely because of the stoichiometric imbalance caused by impurities.

The trimethylstannyl monomer was readily polymerized with a range of 5,5-dibromo-4,4-dialkyl-2,2-bithiophenes in the presence of a palladium catalyst to afford polymers with typical weight average molecular weights (M_w) around 50 000–60 000 g mol^{-1} and polydispersities around 2. Side-chain lengths greater than octyl were necessary to ensure good solubility. Optimization of the cross-coupling conditions demonstrated that the use of bulky phosphine ligands such as tri(o-tolyl)phosphine, resulted in higher molecular weights than for less bulky ligands like triphenylphosphine, most likely due to the suppression of ligand transfer reactions that can occur to the growing polymer chain from less bulky ligands.[89] The use of microwave heating and sealed reaction tubes facilitated the reaction, enabling superheating of the solvent (chlorobenzene) and reducing reaction times from days to minutes.[90] Similar findings have been reported for the use of microwave heating in other polymerizations.[91] Studies were also performed on the effect of end-capping on the polymers physical and electrical properties, since the nature of the end group has been reported to be significant for

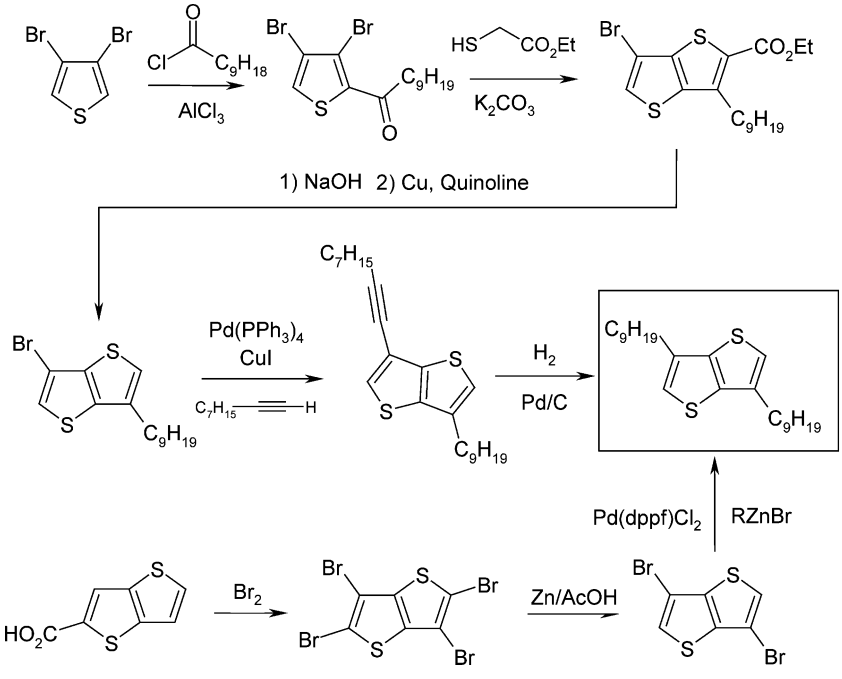

Scheme 2. Two alternative route to 3,6-dialkylthieno[3,2-b]thiophene.

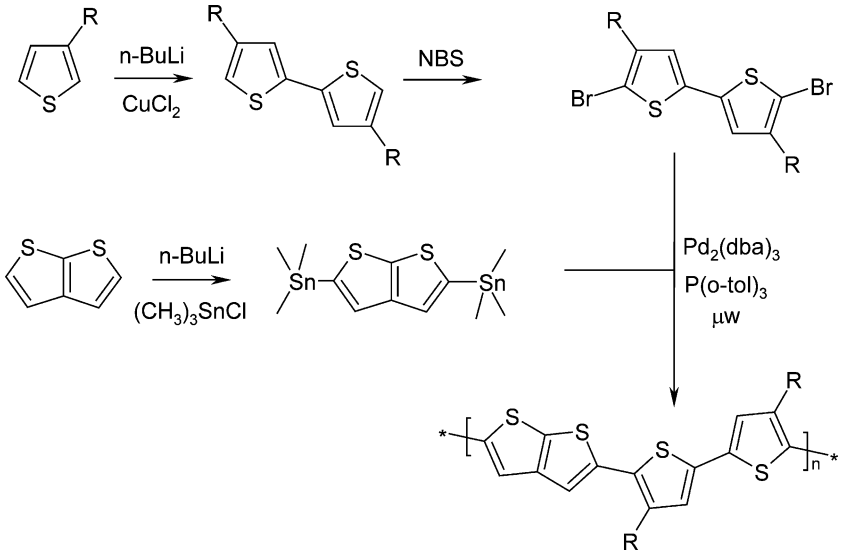

Scheme 3. Synthesis of pBTCT by Stille polymerization.

some polymers.[92] Thus, polymers were endcapped at the end of the polymerization process by the sequential addition of 2-tributylstannylthiophene followed by 2-bromothiophene or bromobenzene. However, no significant differences in the physical or transistor performance for the purified endcapped versus the non-endcapped polymers were apparent.

A similar Stille polymerization strategy afforded both pBTTT[30] and pATBT.[68] For the polymerization of pBTTT, 2,5-trimethyl- (stannyl)thieno[3,2-b]thiophene was utilized as the cross-coupling partner with 5,5-dibromo-4,4-dialkyl-2,2-bithiophenes, whereas for pATBT 2,5-dibromo-3,6-dialkylthienothiophene and 5,5′-bis(trimethyl)stannyl-2,2′-bithiophene were coupled. In both cases molecular weights (M_w) were in the range 50 000–100 000 g mol^{-1} with polydispersities around 2.

Ong and co-workers reported an alternative synthesis of poly(3,6-dipentadecylthieno[3,2-b]thiophene-co-bithiophene) (Scheme 4).[69] In this case a symmetrical monomer was constructed from the Stille cross-coupling of 2,5-dibromo-3,6-dipentadecylthieno[3,2-b]thiophene with 2-tri(butyl)stannylthiophene followed by bromination in the free α positions with N-bromosuccinimide. Dehalogenative polymerization (Yamamoto polymerization[93,94]) was performed by refluxing in toluene in the presence of excess bis(cyclooctadiene)nickel (0) and 2,2′-bipyridyl, to afford the product in 92% yield. The number average molecular mass was 12 400 g mol^{-1} with a polydispersity of 1.6.

Matzger and co-workers[95] reported a further protocol for synthesis of pATBT. In this case, the monomer prepared by the coupling of 2,5-dibromo-3,6-dinonylthieno[3,2-b]thiophene with 2-tri(butyl)stannylthiophene was polymerized directly by oxidative coupling with ferric chloride. The shorter side chains used in this example precluded accurate analysis of the molecular weight by GPC due to poor solubility in the eluting solvent (THF), although the authors did note that the oxidative coupling method afforded higher molecular weight polymer than the same polymer made by the Yamamoto conditions.

It is interesting to compare the thermal properties reported for the same polymer prepared by different polymerization routes. The polymers prepared by the Stille copolymerization (with $C_{12}H_{25}$, $C_{14}H_{29}$ or $C_{16}H_{33}$ sidechains) all exhibited thermotropic LC phase behavior with upper melting temperature in the range of 260–275 °C, whilst that prepared by the Yamamoto polymerization (with pentadecyl sidechains) was semicrystalline with a melting temperature of 148 °C. The thermal behavior for the oxidatively coupled polymer was not reported. The weight average molecular weights of the polymers were 47 000 (C_{12}), 60 000 (C_{14}), and 98 000 (C_{16}) g mol^{-1} for the Stille polymers and 19 500 g mol^{-1} for the Yamamoto. It is unlikely that the change in side chain length is responsible for these differences. A more likely explanation is that the different aspect ratios for the two different polymers are responsible. Ong and co-workers[69] originally compared the thermal behavior of their low weight pATBT to the thermal behavior of high molecular weight pBTTT-C_{14} (mpt 248 °C) and ascribed the large difference in melting behavior to the increased torsional freedom of the unsubstituted bithiophene unit in this backbone of pATBT compared to the substituted bithiophene in pBTTT. The results for the higher weight pATBTs suggest that this is not the case and show that caution must be exercised when comparing seemingly identical polymers of different molecular weight prepared by different polymerization routes.

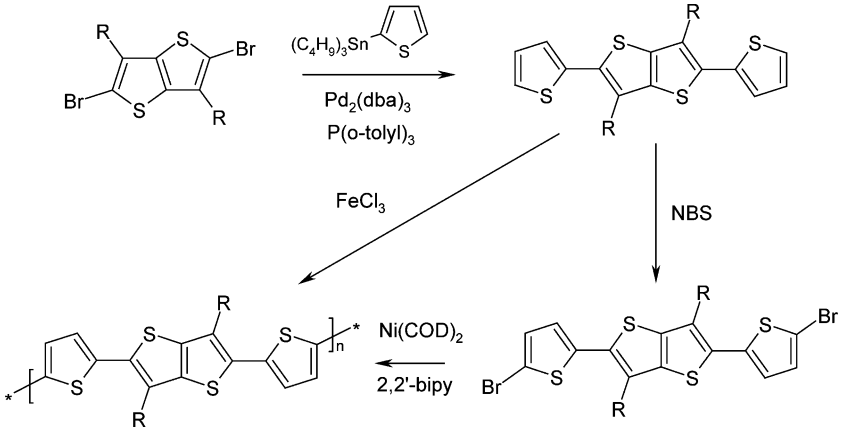

Scheme 4. Synthesis of pATBT by Yamamoto or Oxidative coupling.

Suzuki cross-coupling is a potentially attractive alternative to Stille coupling since it avoids the use of toxic tin reagents. However, typically low degrees of polymerization have been reported during attempts to prepare all-thiophene containing polymers, most likely because of difficulties with deboronation of the thiophene boronic acids or esters during the polymerization[96] and sluggish oxidative addition of the palladium catalyst to the electron rich thiophene during the catalytic cycle.[97] However, the recent development of a range of highly active palladium catalysts with bulky,

electron rich phosphine ligands[98,99] coupled with promising results for the preparation of P3HT,[100] prompted us to investigate the Suzuki polymerization as a route to pBTCT and pBTTT.

The pinacol boron esters of thieno[2,3-b]thiophene and thieno[3,2-b]thiophene were prepared by double lithiation with n-butyl lithium followed by trapping of the resultant anion with 2-isopropoxy-4,4,5,5-tetramethyl-1,3,2-dioxaborolane. These were polymerized with stiochiometric equivalents of 5,5-dibromo-4,4-dialkyl-2,2-bithiophenes in the presence of an aqueous base and palladium catalyst. After screening of several highly active phosphine ligands, we settled upon $Pd(PtBu_3)_2$ as the most active catalyst system.[101] Due to the high air sensitivity of this catalyst, we favored the use of the air stable tetrafluoroborate salt $[HP(^tBu)_3]BF_4$ introduced by Fu,[102] in combination with $Pd_2(dba)_3$. Thus, pBTCT and pBTTT were prepared following the reaction of the appropriate monomers and catalyst in refluxing THF in the presence of aqueous potassium carbonate for 24 h. In some cases additional aliquots of toluene were added during the reaction to prevent precipitation of the polymer. Under these conditions pBTCT-C_{10} with a M_w of 63 000 g mol^{-1} and a polydispersity of 2.1, and pBTTT-C_{12} with a M_w of 48 000 g mol^{-1} and a polydispersity of 1.6 were obtained in yields around 80% after purification. The polymers displayed similar electrical and morphological behavior to those prepared by the Stille polymerization.

12. General Experimental Methods

12.1. Screening Transistor Fabrication and Measurements

Thin-film polymer field-effect transistors were fabricated in a dry nitrogen glove box environment on highly doped silicon substrates with a thermally grown silicon oxide (SiO_2) insulating layer (thickness 230 nm), where the substrate served as a common gate electrode. Transistor source-drain gold contacts were photolithographically defined on the SiO_2 layer with channel lengths L of 2.5, 5, 10, and 20 μm and channel width W of 1 and 2 cm. FET substrates were solvent cleaned and then ozone treated for 10 min in a custom built low-pressure mercury lamp setup. To improve polymer morphology at the interface with the dielectric layer and to passify undesirable polar groups on SiO_2 surface, transistor substrates were treated with silylating agents such as OTS or HMDS. As a result, silica surface was rendered highly hydrophobic with water contact angle between 95° and 105°. Thin semiconductor films were then deposited by spin-coating polymer solutions in organic solvents, including dichlorobenzene and chloroform, onto FET substrates. The samples were then dried and annealed at 100 °C for 10 min for polymers without liquid crystalline phases. For pBTTT transistor thermal treatment was conducted at a wider temperature range coinciding with the on-set of polymer LC smectic phase between 120 and 180 °C. The electrical characterization of the transistor devices was carried out in a dry nitrogen atmosphere using a computer-controlled Agilent 4155C Semiconductor Parameter Analyzer. For air stability measurements samples were removed from the glove box and I-V characteristics were re-measured in the ambient at various time intervals.

Platinum electrode devices are fabricated in a bottom-contact configuration on a degenerately doped n + silicon wafer to be used as a gate. The gate oxide is 200 nm of thermal SiO_2. The source and drain electrodes, patterned by photolithography and a lift-off process, are 40 nm of DC-sputtered Pt with no adhesion layer. The polymer pBTTT-C_{14} was spun-cast from a 3 mg mL^{-1} solution in 1,2-dichlorobenzene at a rate of 3 000 rpm onto substrates rendered hydrophobic by solution treatment with octadecyltrichlorosilane (ODTS). The as-cast films are then heated to 185 °C on a hot plate, followed by a slow cool to room temperature. All processing and device characterization are carried out in an argon-purged glovebox.

13. Summary

Organic electronics is an emerging technology, driven by the steadily improving performance of organic semiconductors in field-effect transistor devices and their ease of processing. This Progress Report has highlighted the structure–property relationships of these materials that have been exploited to achieve high performing devices. Thienothiophene polymers, synthesized carefully to allow optimum molecular weight and low defects or impurities, have been developed as a promising class of solution-processable organic semiconductors. The ability of these polymers to assemble from solution into highly ordered and oriented microstructures that form coherent films is a key element in their performance. Optimization of interfaces, electrodes, environmental exposure, and fabrication conditions all play a role in advancing the performance of the overall devices. Charge carrier mobilities of as high as 1.1 cm^2 V^{-1} s^{-1} have been achieved in optimized device architectures, a value that compares favorably with amorphous silicon devices and provides further momentum for continued development.

Acknowledgements

Portions of this research were carried out at the Stanford Synchrotron Radiation Laboratory, a national user facility operated by Stanford University on behalf of the U.S. Department of Energy, Office of Basic Energy Sciences.

Received: June 17, 2008

[1] P. Horowitz, W. Hill, *The Art of Electronics*, 2nd ed, Cambridge University Press, New York **1990**.
[2] C. D. Dimitrakopoulos, P. R. L. Malenfant, *Adv. Mater.* **2002**, *14*, 99.
[3] J. A. Rogers, K. Baldwin, Z. Bao, B. Crone, A. Dodabalapur, Y. Y. Lin, V. R. Raju, *Proc. Conf. Advanced Metallization 2000, San Diego, CA, United States, Oct.2–5 and University of Tokyo, Tokyo, Japan, Oct. 19–20*, **2000**, 507.
[4] T. Someya, T. Sekitani, S. Iba, Y. Kato, H. Kawaguchi, T. Sakurai, *Proc. Natl. Acad. Sci. U. S. A.* **2004**, *101*, 9966.
[5] A. Facchetti, *Mater. Today* **2007**, *10*, 28.
[6] G. H. Gelinck, H. E. A. Huitema, E. Van Veenendaal, E. Cantatore, L. Schrijnemakers, J. Van der Putten, T. C. T. Geuns, M. Beenhakkers, J. B. Giesbers, B. H. Huisman, E. J. Meijer, E. M. Benito, F. J. Touwslager,

A. W. Marsman, B. J. E. Van Rens, D. M. De Leeuw, *Nat. Mater.* **2004**, *3*, 106.
[7] Y.-L. Loo, *AIChE J.* **2007**, *53*, 1066.
[8] H. Sirringhaus, *Adv. Mater.* **2005**, *17*, 2411.
[9] D. J. Gundlach, J. E. Royer, S. K. Park, S. Subramanian, O. D. Jurchescu, B. H. Hamadani, A. J. Moad, R. J. Kline, L. C. Teague, O. Kirillov, C. A. Richter, J. G. Kushmerick, L. J. Richter, S. R. Parkin, T. N. Jackson, J. E. Anthony, *Nat. Mater.* **2008**, *7*, 216.
[10] M. L. Chabinyc, A. Salleo, *Chem. Mater.* **2004**, *16*, 4509.
[11] S. E. Burns, W. Reeves, B. H. Pui, K. Jacobs, S. Siddique, K. Reynolds, M. Banach, D. Barclay, K. Chalmers, N. Cousins, P. Cain, L. Dassas, M. Etchells, C. Hayton, S. Markham, A. Menon, P. Too, C. Ramsdale, J. Herod, K. Saynor, J. Watts, T. von Werne, J. Mills, C. J. Curling, H. Sirringhaus, K. Amundson, M. D. McCreary, *Dig. Tech. Pap. —Soc. Inf. Disp. Int. Symp.* **2006**, *37*, 74.
[12] Y.-L. Loo, I. McCulloch, *MRS Bulletin* **2008**, *33*, 1.
[13] J. Veres, S. D. Ogier, S. W. Leeming, D. C. Cupertino, S. M. Khaffaf, *Adv. Funct. Mater.* **2003**, *13*, 199.
[14] J. Veres, S. Ogier, G. Lloyd, D. de Leeuw, *Chem. Mater.* **2004**, *16*, 4543.
[15] L. Torsi, A. Dodabalapur, H. E. Katz, *J. Appl. Phys.* **1995**, *78*, 1088.
[16] Y. Xu, P. R. Berger, *J. Appl. Phys.* **2004**, *95*, 1497.
[17] L. Burgi, T. J. Richards, R. H. Friend, H. Sirringhaus, *J. Appl. Phys.* **2003**, *94*, 6129.
[18] R. Hamilton, C. Bailey, W. Duffy, M. Heeney, M. Shkunov, D. Sparrowe, S. Tierney, I. McCulloch, R. J. Kline, D. M. DeLongchamp, M. Chabinyc, *Proc. SPIE—Int. Soc. Opt. Eng.* **2006**, *6336*, 158.
[19] Z. Bao, A. Dodabalapur, A. J. Lovinger, *Appl. Phys. Lett.* **1996**, *69*, 4108.
[20] H. Sirringhaus, P. J. Brown, R. H. Friend, M. M. Nielsen, K. Bechgaard, B. M. W. Langeveld-Voss, A. J. H. Spiering, R. A. J. Janssen, E. W. Meijer, P. Herwig, D. M. de Leeuw, *Nature* **1999**, *401*, 685.
[21] B. H. Hamadani, D. J. Gundlach, I. McCulloch, M. Heeney, *Appl. Phys. Lett.* **2007**, *91*, 243512.
[22] R. S. Loewe, P. C. Ewbank, J. Liu, L. Zhai, R. D. McCullough, *Macromolecules* **2001**, *34*, 4324.
[23] I. A. Liversedge, S. J. Higgins, M. Giles, M. Heeney, I. McCulloch, *Tett. Lett.* **2006**, *47*, 5143.
[24] M. S. A. Abdou, F. P. Orfino, Y. Son, S. Holdcroft, *J. Am. Chem. Soc.* **1997**, *119*, 4518.
[25] R. J. Kline, D. M. DeLongchamp, D. A. Fischer, E. K. Lin, L. J. Richter, M. L. Chabinyc, M. F. Toney, M. Heeney, I. McCulloch, *Macromolecules* **2007**, *40*, 7960.
[26] M. Heeney, C. Bailey, K. Genevicius, M. Shkunov, D. Sparrowe, S. Tierney, I. McCulloch, *J. Am. Chem. Soc.* **2005**, *127*, 1078.
[27] B. M. Medina, A. Van Vooren, P. Brocorens, J. Gierschner, M. Shkunov, M. Heeney, I. McCulloch, R. Lazzaroni, J. Cornil, *Chem. Mater.* **2007**, *19*, 4949.
[28] P. Barta, F. Cacialli, R. Friend, M. Zagorska, *J. Appl. Phys.* **1998**, *84*, 6279.
[29] I. McCulloch, C. Bailey, M. Giles, M. Heeney, I. Love, M. Shkunov, D. Sparrowe, S. Tierney, *Chem. Mater.* **2005**, *17*, 1381.
[30] I. McCulloch, M. Heeney, C. Bailey, K. Genevicius, I. MacDonald, M. Shkunov, D. Sparrowe, S. Tierney, R. Wagner, W. Zhang, M. L. Chabinyc, R. J. Kline, M. D. McGehee, M. F. Toney, *Nat. Mater.* **2006**, *5*, 328.
[31] D. M. DeLongchamp, R. J. Kline, E. K. Lin, D. A. Fischer, L. J. Richter, L. A. Lucas, M. Heeney, I. McCulloch, J. E. Northrup, *Adv. Mater.* **2007**, *19*, 833.
[32] M. L. Chabinyc, M. F. Toney, R. J. Kline, I. McCulloch, M. Heeney, *J. Am. Chem. Soc.* **2007**, *129*, 3226.
[33] B. S. Ong, Y. Wu, P. Liu, S. Gardner, *J. Am. Chem. Soc.* **2004**, *126*, 3378.
[34] L. San Miguel, A. J. Matzger, *Macromolecules* **2007**, *40*, 9233.
[35] Z. Bao, A. J. Lovinger, *Chem. Mater.* **1999**, *11*, 2607.
[36] A. R. Murphy, J. Liu, C. Luscombe, D. Kavulak, J. M. J. Frechet, R. J. Kline, M. D. McGehee, *Chem. Mater.* **2005**, *17*, 4892.
[37] R. J. Kline, M. D. McGehee, E. N. Kadnikova, J. Liu, J. M. J. Frechet, *Adv. Mater.* **2003**, *15*, 1519.
[38] R. J. Kline, M. D. McGehee, E. N. Kadnikova, J. Liu, J. M. J. Frechet, M. F. Toney, *Macromolecules* **2005**, *38*, 3312.
[39] A. Zen, J. Pflaum, S. Hirschmann, W. Zhuang, F. Jaiser, U. Asawapirom, J. P. Rabe, U. Scherf, D. Neher, *Adv. Funct. Mater.* **2004**, *14*, 757.
[40] R. Pokrop, J.-M. Verilhac, A. Gasior, I. Wielgus, M. Zagorska, J.-P. Travers, A. Pron, *J. Mater. Chem.* **2006**, *16*, 3099.
[41] J.-M. Verilhac, R. Pokrop, G. LeBlevennec, I. Kulszewicz-Bajer, K. Buga, M. Zagorska, S. Sadki, A. Pron, *J. Phys. Chem. B* **2006**, *110*, 13305.
[42] J.-F. Chang, J. Clark, N. Zhao, H. Sirringhaus, D. W. Breiby, J. W. Andreasen, M. M. Nielsen, M. Giles, M. Heeney, I. McCulloch, *Phys. Rev. B* **2006**, *74*, 115318.
[43] M. Brinkmann, P. Rannou, *Adv. Funct. Mater.* **2007**, *17*, 101.
[44] A. Salleo, M. L. Chabinyc, M. Yang, R. Street, *Appl. Phys. Lett.* **2002**, *81*, 4383.
[45] R. J. Kline, D. M. DeLongchamp, D. A. Fischer, E. K. Lin, M. Heeney, I. McCulloch, M. F. Toney, *Appl. Phys. Lett.* **2007**, *90*, 062117.
[46] L. Chabinyc Michael, F. Toney Michael, R. J. Kline, I. McCulloch, M. Heeney, *J. Am. Chem. Soc.* **2007**, *129*, 3226.
[47] M. L. Chabinyc, R. Lujan, F. Endicott, M. F. Toney, I. McCulloch, M. Heeney, *Appl. Phys. Lett.* **2007**, *90*, 233508/1.
[48] T. J. Prosa, M. J. Wimokur, J. Moulton, P. Smith, A. J. Heeger, *Macromolecules* **1992**, *25*, 4364.
[49] P. Brocorens, J. Cornil, M. L. Chabinyc, M. F. Toney, M. Shkunov, M. Heeney, I. McCulloch, R. Lazzaroni, *Adv. Mater.* **2009**, DOI:10.1002/adma.200801668.
[50] J. Stöhr, *NEXAFS Spectroscopy, Springer Series in Surface Science Vol. 392*, Springer, Berlin **1992**.
[51] a) J. E. Northrup, *Phys. Rev. B: Condens. Matter Mater. Phys.* **2007**, *76*, 245202/1. b) A. Salleo, personal communication.
[52] J. E. Anthony, *Chem. Rev.* **2006**, *106*, 5028.
[53] A. Zen, M. Saphiannikova, D. Neher, U. Asawapirom, U. Scherf, *Chem. Mater.* **2005**, *17*, 781.
[54] A. Babel, S. A. Jenekhe, *Synth. Met.* **2005**, *148*, 169.
[55] Z. Bao, Y. Feng, A. Dodabalapur, V. R. Raju, A. J. Lovinger, *Chem. Mater.* **1997**, *9*, 1299.
[56] X. Zhang, M. Koehler, A. J. Matzger, *Macromolecules* **2004**, *37*, 6306.
[57] M. Turbiez, P. Frere, P. Leriche, N. Mercier, J. Roncali, *Chem. Comm.* **2005**, 1161.
[58] N. Hergue, P. Frere, *Org. Biomol. Chem.* **2007**, *5*, 3442.
[59] E. Lim, B. J. Jung, J. Lee, H. K. Shim, J. I. Lee, Y. S. Yang, L. M. Do, *Macromolecules* **2005**, *38*, 4531.
[60] E. Lim, B. J. Jung, H. K. Shim, *Macromolecules* **2003**, *36*, 4288.
[61] W. H. Tang, L. Ke, L. W. Tan, T. T. Lin, T. Kietzke, Z. K. Chen, *Macromolecules* **2007**, *40*, 6164.
[62] M. C. Gather, M. Heeney, W. Zhang, K. S. Whitehead, D. C. C. Bradley, I. McCulloch, A. J. Campbell, *Chem. Commun.* **2008**, 1079.
[63] E. Lim, Y. M. Kim, J. I. Lee, B. J. Jung, N. S. Cho, J. Lee, L. M. Do, H. K. Shim, *J. Pol. Sci. A. Poly. Chem.* **2006**, *44*, 4709.
[64] H. Sirringhaus, R. J. Wilson, R. H. Friend, M. Inbasekaran, W. Wu, E. P. Woo, M. Grell, D. D. C. Bradley, *Appl. Phys. Lett.* **2000**, *77*, 406.
[65] Y. M. Kim, E. Lim, I.-N. Kang, B.-J. Jung, J. Lee, B. W. Koo, L.-M. Do, H.-K. Shim, *Macromolecules* **2006**, *39*, 4081.
[66] S. Tierney, C. Bailey, W. Duffy, R. Hamilton, M. Heeney, I. MacDonald, M. Shkunov, D. Sparrowe, W. Zhang, I. McCulloch, *PMSE Preprints* **2007**, *96*, 180.
[67] M. Heeney, R. Wagner, I. McCulloch, S. Tierney, *WO2005111045*, **2005**.
[68] M. Heeney, C. Bailey, W. Duffy, M. Shkunov, D. Sparrowe, S. Tierney, W. Zhang, I. McCulloch, *PMSE Preprints* **2006**, *95*, 101.
[69] Y. N. Li, Y. L. Wu, P. Liu, M. Birau, H. L. Pan, B. S. Ong, *Adv. Mater.* **2006**, *18*, 3029.

[70] J. E. Northrup, M. L. Chabinyc, R. Hamilton, I. McCulloch, M. Heeney, *J. Appl. Phys.* **2008**, 104.
[71] M. Heeney, C. Bailey, S. Tierney, I. McCulloch, *WO2006021277*, **2006**.
[72] B. H. Hamadani, C. A. Richter, D. J. Gundlach, R. J. Kline, I. McCulloch, M. Heeney, *J. Appl. Phys.* **2007**, *102*, 044503/1.
[73] T. Kreouzis, D. Poplavskyy, S. M. Tuladhar, M. Campoy-Quiles, J. Nelson, A. J. Campbell, D. D. C. Bradley, *Phys. Rev. B: Condens. Matter Mater. Phys.* **2006**, *73*, 235201/1.
[74] D. M. de Leeuw, M. M. J. Simenon, A. R. Brown, R. E. F. Einerhand, *Synth. Met.* **1997**, *87*, 53.
[75] E. J. Meijer, C. Detcheverry, P. J. Baesjou, E. van Veenendaal, D. M. de Leeuw, T. M. Klapwijk, *J. Appl. Phys.* **2003**, *93*, 4831.
[76] M. Chabinyc, R. A. Street, J. E. Northrup, Appl. Phys. Lett., **2007**, *90*, 123508.
[77] H. Rost, J. Ficker, J. S. Alonso, L. Leenders, I. McCulloch, *Synth. Met.* **2004**, *145*, 83.
[78] M. H. Yoon, S. A. DiBenedetto, A. Facchetti, T. J. Marks, *J. Am. Chem. Soc.* **2005**, *127*, 1348.
[79] T. Umeda, S. Tokito, D. Kumaki, *J. Appl. Phys.* **2007**, *101*, 054517.
[80] W. J. Archer, R. Taylor, *J. Chem. Soc. Perkin Trans. 2* **1982**, 295.
[81] T. Otsubo, Y. Kono, N. Hozo, H. Miyamoto, Y. Aso, F. Ogura, T. Tanaka, M. Sawada, *Bull. Chem. Soc. Jpn.* **1993**, *66*, 2033.
[82] S. Yasuike, J. Kurita, T. Tsuchiya, *Heterocycles* **1997**, *45*, 1891.
[83] M. Heeney, C. Bailey, K. Genevicius, M. Giles, M. Shkunov, D. Sparrowe, S. Tierney, W. Zhang, I. McCulloch, *Proc. SPIE-Int. Soc. Opt. Eng. FIELD* **2005**, *5940*, 594007/1.
[84] B. L. Chenard, R. L. Harlow, A. L. Johnson, S. A. Vladuchick, *J. Am. Chem. Soc.* **1985**, *107*, 3871.
[85] R. Cagnoli, M. Lanzi, A. Mucci, F. Parenti, L. Schenetti, *Synthesis* **2005**, 267.
[86] P. Leriche, J. M. Raimundo, M. Turbiez, V. Monroche, M. Allain, F. X. Sauvage, J. Roncali, P. Frere, P. J. Skabara, *J. Mater. Chem.* **2003**, *13*, 1324.
[87] D. W. Hawkins, B. Iddon, D. S. Longthorne, P. J. Rosyk, *J. Chem. Soc. Perkin Trans. 1* **1994**, 2735.
[88] L. S. Fuller, B. Iddon, K. A. Smith, *J. Chem. Soc.* **1997**, 3465.
[89] F. E. Goodson, T. I. Wallow, B. M. Novak, *Macromolecules* **1998**, *31*, 2047.
[90] S. Tierney, M. Heeney, I. McCulloch, *Synth. Met.* **2005**, *148*, 195.
[91] F. Galbrecht, T. W. Bunnagel, U. Scherf, T. Farrell, *Macromol. Rapid Comm.* **2007**, *28*, 387.
[92] Y. Kim, S. Cook, J. Kirkpatrick, J. Nelson, J. R. Durrant, D. D. C. Bradley, M. Giles, M. Heeney, R. Hamilton, I. McCulloch, *J. Phys. Chem. C* **2007**, *111*, 8137.
[93] T. Yamamoto, *J. Organomet. Chem.* **2002**, *653*, 195.
[94] T. Yamamoto, A. Morita, Y. Miyazaki, T. Maruyama, H. Wakayama, Z. Zhou, Y. Nakamura, T. Kanbara, S. Sasaki, K. Kubota, *Macromolecules* **1992**, *25*, 1214.
[95] L. S. Miguel, A. J. Matzger, *Macromolecules* **2007**, *40*, 9233.
[96] M. Jayakannan, J. L. J. van Dongen, R. A. J. Janssen, *Macromolecules* **2001**, *34*, 5386.
[97] S. Guillerez, G. Bidan, *Synth. Met.* **1998**, *93*, 123.
[98] F. Bellina, A. Carpita, R. Rossi, *Synthesis*, **2004**, *15*, 2419.
[99] S. Kotha, A. K. Ghosh, *Synlett.* **2002**, 451.
[100] I. A. Liversedge, S. J. Higgins, M. Giles, M. Heeney, I. McCulloch, *Tett. Lett.* **2006**, *47*, 5143.
[101] S. Tierney, M. Heeney, W. Zhang, S. Higgins, I. Liversedge, *EP* 1754736, **2007**.
[102] M. R. Netherton, G. C. Fu, *Org. Lett.*, **2001**, *3*, 4295.